THE ASTROPHYSICAL JOURNAL, 448:98–118, 1995 July 20

AN X-RAY AND OPTICAL STUDY OF THE DWARF GALAXY NGC 1569: EVIDENCE FOR A STARBURST-DRIVEN OUTFLOW

TIMOTHY M. HECKMAN[1,2] AND MICHAEL DAHLEM[3]
Department of Physics and Astronomy, Johns Hopkins University, Baltimore, MD 21218
MATTHEW D. LEHNERT[2]
Institute for Geophysics and Planetary Physics, Lawrence Livermore National Laboratory, P.O. Box 808, L-413, Livermore, CA 94551-9900
GIUSEPPINA FABBIANO
Harvard-Smithsonian Center for Astrophysics, 60 Garden Street, Cambridge, MA 02138
DIANE GILMORE
Space Telescope Science Institute, 3700 San Martin Drive, Baltimore, MD 21218
AND
WILLIAM H. WALLER
Hughes STX Corporation, Laboratory for Astronomy and Solar Physics, NASA/Goddard Space Flight Center, Greenbelt, MD 20771
Received 1994 September 8; accepted 1995 January 30

ABSTRACT

Supernova-driven outflows produced by intense bursts of star formation can drastically affect the structure and subsequent evolution of dwarf galaxies. Extensive mass loss from such systems may also provide an important source of chemical enrichment for the intergalactic medium. Despite the potential importance of these outflows, there is a very limited amount of direct observational evidence for their existence. One of the clearest signatures of a starburst-driven outflow is the X-ray emission from the hot gas that drives the outflow. We have therefore undertaken an X-ray imaging and optical spectroscopic investigation of the nearest and best-studied starbursting dwarf galaxy NGC 1569 using the HRI on *ROSAT* and the Ritchey-Chrétien spectrograph on the KPNO 4 m telescope, respectively. We find that at least half the keV X-ray emission of NGC 1569 is associated with a diffuse halo that is some 3.8 × 2.2 ~ 2.4 × 1.5 kpc in size. Kiloparsec-scale "spurs" of diffuse X-ray emission extend outward along or near the optical minor axis of the galaxy. These diffuse X-ray spurs are morphologically associated with the well-known system of Hα filaments. Previous kinematic studies have suggested that the Hα filament system is a bipolar outflow. Our new optical spectroscopic data show that the Hα emission comprises two kinematically distinct components: a quiescent system about 1 kpc in size responsible for about 75% of the Hα emission and a fainter and more complex system over 2 kpc in size with radial velocities of as much as ± 200 km s^{-1} relative to v_{sys}. The latter appears to define expanding hollow structures consisting of several kiloparsec-scale "superbubbles." The dynamical age of the high-velocity system ($\sim 10^7$ yr) is similar to various estimates of the age of the starburst. We also see very broad wings (full width at zero intensity of 1400–2300 km s^{-1}) on the Hα emission-line profile at the location of super starcluster A, suggestive of recent supernova activity there.

We argue that the starburst in NGC 1569 is driving an outflow of the interstellar medium on a global scale. Our simple models suggest that the X-ray emission is too bright to come primarily from the hot tenuous supernova-heated gas in the interior of a superbubble, unless this gas is evaporating or ablating cool dense material. This latter material may be the outer shell of the superbubble or interstellar clouds that have been engulfed by the superbubble. The high-velocity Hα filaments probably correspond to the shocked and accelerated ambient material in the superbubble's outer walls, while the low-velocity material may be massive photoionized clouds in the starbursting galactic disk. The observed expansion speeds probably exceed the galactic escape velocity. It seems likely that the expanding material will ultimately "blow out" of the interstellar medium, and in so doing may allow most of the metals created by the starburst to escape from the galaxy. It is less clear whether the outflow will lead to the ejection of most or all of this galaxy's interstellar medium, though it appears at least energetically feasible. We briefly discuss the significance of these results for ideas about the evolution of dwarf galaxies.

Subject headings: galaxies: halos — galaxies: individual (NGC 1569) — galaxies: kinematics and dynamics — galaxies: starburst — X-rays: galaxies

[1] Adjunct Astronomer, Space Telescope Science Institute.
[2] Visiting Astronomer, Kitt Peak National Observatory of the National Optical Astronomy Observatories, operated by AURA, Inc., under contract with the National Science Foundation.
[3] Present address: Space Telescope Science Institute, 3700 San Martin Drive, Baltimore, MD 21218.

1. INTRODUCTION

Dwarf galaxies are potentially important in many contexts in current ideas about galaxy evolution and cosmology. They may represent the sites of the earliest star formation in the universe and the basic building blocks for larger galaxies (see White & Frenk 1991). They may make a significant contribution to the cosmic X-ray background (see Griffiths & Padovani 1990) and could be related to the Lyα forest absorption-line systems at high redshift (e.g., Bond, Szalay, Silk 1988). At moderate redshifts, starbursting low-mass galaxies dominate the faint galaxy counts in the blue and (unlike the situation for more luminous galaxies like our own) have apparently undergone very strong evolution in the recent past (see Broadhurst, Ellis, & Glazebrook 1992; Lilly 1993; Steidel 1993). Dwarf galaxies also represent ideal laboratories for testing various ideas about galaxy evolution and the interstellar medium, since they are thought to be rather simple systems that are at the same time fragile, and hence likely to be strongly affected by both external and internal processes (see Sandage & Binggeli 1984; Gallagher & Hunter 1984; Bothun et al. 1986).

Perhaps the most widely discussed such process in dwarfs is the generation of a starburst-driven galactic wind (e.g., Sandage 1965; Larson 1974; Larson & Dinerstein 1975; Saito 1979; Silk, Wyse, & Shields 1987; Vader 1986, 1987; Hensler & Burkert 1990). During and shortly after a centrally concentrated starburst, the kinetic energy supplied by supernovae and stellar winds is predicted to inflate an expanding "superbubble" in the surrounding interstellar medium of a dwarf galaxy (see McLow & McCray 1988; Tenario-Tagle & Bodenheimer 1988; Koo & McKee 1992). The outer shell of the bubble (consisting of swept-up ambient gas) probably corresponds to the optical emission-line loops and filaments that are present in many such galaxies (see Marlowe et al. 1995, hereafter MHWS; Meurer et al. 1992). The hot gaseous "piston" in the interior of the superbubble—consisting of the metal-rich thermalized ejecta of supernovae and stellar winds, plus material evaporated or ablated off interstellar clouds—should be a source of thermal keV X-rays (see Mac Low & McCray 1988). Given a sufficiently energetic and long-lasting starburst, the superbubble may ultimately "blow out" of the dwarf's interstellar medium (ISM) and its outer shell can then fragment, so that the hot outrushing gas can then develop into a full-fledged galactic wind (e.g., Chevalier & Clegg 1985; Heckman, Lehnert, & Armus 1993; Suchkov et al. 1994).

Such an outflow is hypothesized to have a particularly devastating impact on a dwarf galaxy because the dwarf's relatively low escape velocity will facilitate the removal of substantial amounts of interstellar matter. If mass loss is indeed a by-product of vigorous star formation in dwarf galaxies, it could explain many of the otherwise puzzling properties of dwarfs. Their low metallicities would then be the result of their inability to retain newly synthesized metals (see De Young & Gallagher 1990), while the metals lost from dwarf galaxies may comprise a substantial fraction of the metals currently in the intergalactic medium (see Lynden-Bell 1992). The low surface brightnesses of most dwarfs could result from both the expansion of the dwarf following the loss of a substantial fraction of its mass, and the cessation of star formation resulting from the loss of its ISM. This "destruction" (or at least, dramatic fading) of dwarfs might be related to the strong evolution of the faint galaxy population noted above (e.g., Babul & Rees 1992). Finally, wind-driven mass loss may be able to transmute one type of dwarf galaxy into another (e.g., Faber & Lin 1983; Kormendy 1985).

Despite its potential importance, the process of starburst-driven mass loss in dwarf galaxies has only recently begun to be studied observationally. The pioneering study of NGC 1705 (Meurer 1989; Meurer et al. 1992) is particularly noteworthy and has been followed up by MHWS, who observed a large sample of starbursting dwarf amorphous galaxies and found optical evidence for outflows in about half of them. While X-ray emission may offer the best opportunity to detect and study such outflows, heretofore no dwarf starburst galaxies have been investigated in sufficient detail at X-ray wavelengths to convincingly establish the presence of hot outflowing gas.

NGC 1569—as probably the nearest and best-studied example of a dwarf starburst galaxy—is an ideal laboratory for testing our ideas about the role of starbursts in the evolution of dwarf galaxies and about the physics of starburst-driven outflows (see Israel 1988; Waller 1991; O'Connell, Gallagher, & Hunter 1994; Drissen, Roy, & Moffat 1993). The relevant properties of this galaxy are summarized in Table 1. At our assumed distance of 2.2 Mpc (Israel 1988—but see Hunter & Gallagher 1986), NGC 1569 has an absolute blue magnitude of $M_B = -17 (L_B = 10^9\ L_\odot = 6\% L_*)$ and a mass of only about $3.4 \times 10^8\ M_\odot$ (of which about half is gas). Its extremely blue colors, luminous Hα emission, strong, warm IR emission, "super star clusters," and relatively short inferred gas depletion timescale all imply that NGC 1569 is in an unusual evolutionary state dominated by a substantial population of young, high-mass stars. The properties of its two super star clusters,

TABLE 1

GLOBAL PROPERTIES OF NGC 1569

D (1)	M_B (2)	$(U-B)$ (3)	$(B-V)$ (4)	L_x (5)	L_{bol} (6)	$L_{H\alpha}$ (7)	$E_{H\alpha}$ (8)	M_{gas} (9)	M_{tot} (10)	[O/H] (11)	N(H I) (12)
2.2	−17.1	−0.62	0.23	38.8	42.9	40.7	160	8.2	8.5	−0.6	21.3

NOTES.—Col. (1): Assumed distance in Mpc (Israel 1988); cols. (2)–(4): Absolute blue magnitude, $(U-B)$ color, and $(B-V)$ color corrected for Galactic extinction (Israel 1988); col. (5): log of the 0.1–2.4 keV X-ray luminosity in ergs s^{-1} assuming our standard "warm thermal model" (see text for details); col. (6): log of the bolometric (UV plus optical plus IR) luminosity in ergs s^{-1} (Israel 1988); col. (7): log of the Hα luminosity in ergs s^{-1} corrected for Galactic extinction. This is the average of the values given in Hunter, Hawley, & Gallagher 1993, Waller 1991, and Kennicutt & Kent 1983; col. (8): The global equivalent width of the Hα emission line in Å. This is the average of the values given in Kennicutt & Kent 1983, Waller 1991, and Kennicutt 1992; col. (9): log of the mass of neutral and molecular gas (H I, He I, H_2) in solar masses (Israel 1988); col. (10): log of the total dynamical mass within a radius of 1.3 kpc in $M_\odot$ (Reakes 1980); col. (11): log of the oxygen abundance relative to solar. This is the mean of the values given by Hunter et al. 1982, Skillman, Kennicutt, & Hodge 1989, and Storchi-Bergman, Kinney, & Calzetti 1994; col. (12): log of the foreground (Galactic) H I column density in cm^{-2} (D. Hartmann, private communication).

the high-frequency cutoff in its nonthermal radio spectrum, and the relative paucity of early type O and Wolf-Rayet stars have led to the idea that it is in a "postburst" phase some $\sim 10^7$ yr after the peak star-formation rate. Thus, a very high rate of energy injection by supernovae is expected (see Leitherer & Heckman 1995), since the least massive Type II supernova progenitors have lifetimes of about 40–50 Myr.

Hodge (1974), Waller (1991), and Hunter, Hawley, & Gallagher (1993) have presented deep Hα images of NGC 1569, showing that it is immersed in a bright and morphologically complex system of emission-line filaments and loops that extend out several kpc preferentially along the minor axis of the galaxy. The kinematics of this gas was investigated by de Vaucouleurs, de Vaucouleurs, & Pence (1974) and de Vaucouleurs (1981), who suggested that the gas was being expelled on a timescale of about 10 Myr in a bipolar outflow directed along the optical minor axis at $v \sim 100$ km s^{-1}. More recently, multiple slit spectroscopy of the main body of NGC 1569 by Tomita, Ohta, & Saito (1994, hereafter TOS) has revealed kinematic evidence for several expanding bubble-like structures with typical sizes of a few hundred pc and expansion velocities of up to 50 km s^{-1}. Finally, NGC 1569 was detected as a moderately strong (and possibly spatially resolved) X-ray source by the *Einstein Observatory*'s IPC (Fabbiano, Feigelson, & Zamorani 1982; Fabbiano, Kim, & Trinchieri 1992).

We have therefore observed NGC 1569 with the HRI on board *ROSAT*, and have also obtained long-slit optical spectroscopic data using the Ritchey-Chrétien spectrograph on the KPNO 4 m telescope with the following specific aims.

1. Determine the fraction of X-ray emission in NGC 1569 that arises in a diffuse, spatially extended nebula (consistent with a wind or wind-blown superbubble), rather than with discrete compact sources in the starburst itself (massive X-ray binaries and individual supernova remnants).
2. Determine the size, morphology, and luminosity of the diffuse X-ray emission and compare them to models of X-ray emission from galactic winds and wind-blown superbubbles (e.g., Tomisaka & Ikeuchi 1988; Tomisaka & Bregman 1993; Suchkov et al. 1994).
3. Relate the diffuse X-ray emission to the Hα filament system both morphologically and physically.
4. Further elucidate the kinematics of the Hα filament system, compare these kinematics to models of expanding superbubbles, and relate the dynamics of the filaments to the properties of the hot X-ray–emitting gas.
5. Estimate or meaningfully constrain the pressures and the kinetic/thermal energy content of both the X-ray–emitting gas and the Hα filament system. These parameters are important for evaluating the total energy budget of an outflow.
6. Relate the overall dynamical state of the hot and warm interstellar medium in this galaxy to the stellar content and recent evolutionary history of the galaxy.
7. Attempt to predict the long-term impact of the starburst on the ISM of NGC 1569 and on the subsequent evolution of the galaxy.

In § 2 we will discuss the analysis of the X-ray data and the results we have gleaned from this. We will similarly discuss the optical spectroscopy in § 3. Our new results will be discussed in the context of models for starbursts and starburst-driven outflows in § 4. The major results, and their implications for the issues summarized above, will be presented in § 5.

2. THE X-RAY DATA

2.1. *Observations and Data Analysis*

We have observed NGC 1569 with the *ROSAT* High Resolution Imager (HRI) for a total of 11.268 ks on 1992 March 14–15. The HRI is described in detail by David et al. (1993). When combined with the *ROSAT* X-Ray Telescope (XRT), the peak effective area of the HRI is about 95 cm^2 at 1.1 keV, and the effective area is greater than 40 cm^2 between 0.7 and 1.7 keV.

2.1.1. *Image Processing*

The HRI + XRT on-axis point spread function (PSF) consists of a narrow core which has a full width half-maximum (FWHM) of about 5″ and contains about 40% of the total encircled energy, and broad wings (such that about 15% of the encircled energy is scattered beyond 10″ and 5% is scattered beyond 1′). The PSF begins to degrade significantly for angles off-axis of more than about 7′, but all the detected X-ray emission associated with NGC 1569 is located within about 3′ of the field center.

Five stars near NGC 1569, at projected distances less than 6′, could be identified in our HRI image. We used these stars to determine a correction to the nominal position of the field center of the *ROSAT* pointing during the observation of NGC 1569. The applied correction amounts to just less than 2″ to the northeast. The positional accuracy after this correction is better than 2″, based on consistency between the five stars.

We determined the background level of the observation by calculating the mean count rates in three source-free regions of the sky close to NGC 1569. The results for these three regions were very similar, showing that the background near this galaxy is rather homogeneous. The mean value of the background was 0.013 counts arcsec^{-2}, and this constant value was subtracted from the data before measuring the counts for the sources associated with NGC 1569.

For the final display, we rebinned the image to 1.″5 × 1.″5 pixels (i.e., 3 × 3 original HRI pixels). To improve the signal-to-noise ratio, the data were first slightly smoothed with a Gaussian gaving a σ of 1 pixel, or a FWHM $\sim$ 3.″5. This image effectively preserves the intrinsic FWHM of the HRI + XRT PSF of about 5″ (it has an effective resolution of about 6″). We also produced a slightly lower resolution image by smoothing with a Gaussian having a σ of two pixels (FWHM $\sim$ 7″), implying an effective resolution of about 8.″6 FWHM. Finally, in order to display the diffuse, low–surface-brightness emission we produced a low-resolution image. We first removed the two strongest point sources in NGC 1569 (see § 2.2 below) by using the on-axis HRI + XRT PSF as described in David et al. (1993). For this purpose, the PSF profile was centered on each of the emission profiles of the two sources and scaled to their observed intensities. After removal of the counts contributed by these sources, the data were smoothed with a Gaussian having a σ of 10 pixels. The effective resolution of this image is about 36″ FWHM.

2.1.2. *Conversion to Fluxes*

To convert an HRI count rate into a flux requires adopting a specific model for the X-ray emission. While the standard *ROSAT* bandpass is 0.1–2.4 keV (and this is the range for which the conversions from counts s^{-1} to ergs cm^{-2} s^{-1} are given for the HRI by David et al. 1993), as noted above, the HRI has a relatively large effective area only over the relatively narrow energy range between 0.7 and 1.7 keV. Moreover, the

large foreground Galactic H I column ($N_H = 2.1 \times 10^{21}$ cm^{-2}) corresponds to optical depths of $\tau = 1$ at 0.7 keV and $\tau = 2.5$ at 0.4 keV. Thus, our data really provide very little direct information about the X-ray properties of NGC 1569 at energies much below 0.7 keV.

Keeping this caveat in mind, we will quote fluxes in the standard 0.1–2.4 keV *ROSAT* band. To do so, we have first adopted the Galactic H I column given above, taken several different physically plausible models for the X-ray emission, and then used the tables of energy conversion factors (ECFs) in David et al. (1993) to convert HRI counts s^{-1} into ergs cm^{-2} s^{-1}. Very recent X-ray observations of NGC 1569 with ASCA (R. Della Ceca, private communication) show that its X-ray spectrum is complex. A warm thermal source with $kT \approx 0.8$ keV dominates the X-ray emission in the energy range between about 0.7 and 1.3 keV. At higher energies, a hard thermal or nonthermal source dominates. There is no evidence for an absorbing column in excess of the Galactic value (see above).

The corresponding *ROSAT* HRI ECFs in David et al. (1993) are then 0.087×10^{11} counts cm^2 ergs^{-1} for thermal plasma with $kT = 0.8$ keV, 0.064×10^{11} counts cm^2 ergs^{-1} for thermal plasma with $kT = 5$ keV, and 0.051×10^{11} counts cm^2 ergs^{-1} for a nonthermal source with a canonical photon index of 1.7. The ASCA observations suggest that the soft thermal source provides most of the emission from the large X-ray halo (see below), and we will therefore use the ECF for $kT = 0.8$ keV in the rest of the paper, except where explicitly noted.

The ECFs given above apply to a point source as measured through a 5″ × 5″ square aperture and assume that this small aperture contains only half the total counts for a point source. We have, therefore, followed this procedure and definition for calculating fluxes from point source. However, for diffuse sources (where we have used much larger apertures that contain essentially all the counts) we have first multiplied the adopted EXF by two before calculating fluxes, thus removing the "aperture correction" from the adopted ECF.

2.2. *Results*

Our HRI image of NGC 1569 is shown in Figure 1*a* after smoothing slightly to an effective resolution (FWHM) of 6″ = 64 pc (hereafter the "full-resolution" image), in Figure 1*b* (Plate 1) after smoothing to an effective resolution of 8.″6 = 92 pc (the "high-resolution" image), and in Figure 1*c* (Plate 2) after smoothing to an effective resolution of 36″ = 380 pc (the "low-resolution" image). In Figures 1*b* and 1*c*, these contour plots of the X-ray emission have been overlain on gray-scale representations of a continuum-subtracted narrow-band image of the Hα emission kindly provided by D. Hunter (and published in Hunter et al. 1993).

The basic X-ray properties of NGC 1569 are summarized in Table 2. We detect a total of 167 ± 25 net counts within a radius of 1.′9 in 11.268 ks, for a total count rate of 0.0148 ± 0.0022 s^{-1}, where the uncertainty is the square root of the gross counts (source plus background). The implied fluxes in the 0.1–2.4 keV band are then $8.6 \pm 1.3 \times 10^{-13}$, $1.2 \pm 0.2 \times 10^{-12}$, and $1.4 \pm 0.2 \times 10^{-12}$ ergs cm^{-2} s^{-1} for the warm thermal model ($kT = 0.8$ keV), the hot thermal model ($kT = 5$ keV), and the nonthermal power-law model ($\Gamma = 1.7$), respectively. Note that these represent the fluxes after correction for attenuation corresponding to our adopted value of N_H (i.e., they are the unobscured fluxes "outside the Galaxy"). For our adopted distance of 2.2 Mpc, the total lumi-

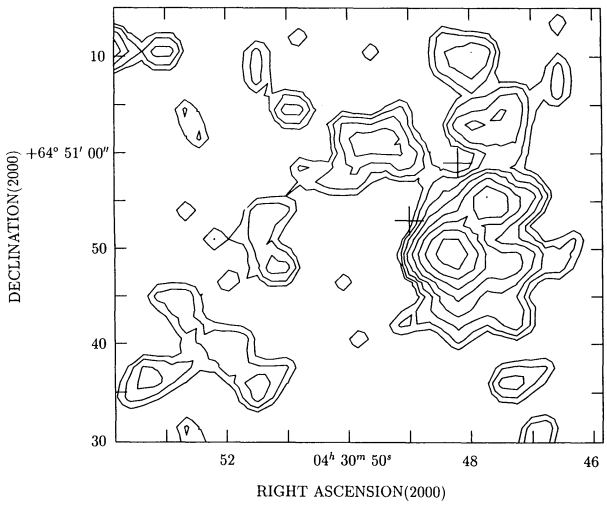

FIG. 1*a*

FIG. 1.—(*a*) The full-resolution *ROSAT* HRI image (effective resolution 6″ FWHM). The size of the region displayed is 52.″5 × 45″, and the contours are at levels of 0.044 (3.5 σ), 0.062, 0.089, 0.124, 0.178, 0.254, 0.356, and 0.489 counts arcsec^{-2} above the background. The positions of the super star clusters A and B (Ables 1971) are indicated by crosses. (*b*) Overlay of our *ROSAT* HRI high-resolution image (8.″6 FWHM) in contour form on a gray-scale representation of a continuum-subtracted Hα image kindly provided by D. Hunter (published in Hunter, Hawley, & Gallagher 1993). The HRI contours are at levels of 0.022 (2.5 σ), 0.031, 0.044, 0.063, 0.088, ..., 0.252 counts arcsec^{-2} above the background. (*c*) Same as (*b*), but showing our low-resolution HRI image (36″ FWHM). Prior to smoothing the original HRI image, we have subtracted the two point sources (sources 1 and 2) using an appropriately scaled HRI + XRT PSF (see text for details). X-ray emission from a bright star is responsible for the contours at the lower left edge of the figure. The HRI contours are at levels of 0.0036 (2 σ), 0.0054, 0.0072, ..., 0.036 counts arcsec^{-2} above the background.

TABLE 2

OBSERVED X-RAY PROPERTIES

Region (1)	Counts (2)	F_x (3)	L_x (4)	Size (5)
Source 1.....	16 ± 4	1.6	1.0	<5″(<43 pc)
Source 2.....	8 ± 3	0.8	0.5	<5″(<43 pc)
Ridge	33 ± 7	1.7	1.0	45″ × 20″(480 pc × 210 pc)
Halo	86 ± 26	4.4	2.6	3.′8 (2.4 kpc)
S Blob.....	23 ± 9	1.2	0.7	1′ (0.6 kpc)
Total	190 ± 27	9.7	5.7	4′ (2.6 kpc)

NOTES.—Col. (1): See text; col. (2): For Sources 1 and 2 these are the counts in a 5″ × 5″ box, while for the other sources the counts are measured in apertures with sizes given in col. (5). The *ROSAT* HRI PSF has broad wings, so that a 5″ × 5″ box contains only about half the total counts contributed by sources (see text and David et al. 1993). The error bars assume Poisson statistics (they are the square root of the source + background counts in the photometric aperture). Col. (3): Fluxes in the *ROSAT* 0.1–2.4 keV band in units of 10^{-13} ergs cm^{-2} s^{-1}. These are calculted from the counts in col. (2), the integration time of 11.268 ks, and the energy conversion factor (ECF) of 1 ergs cm^{-2} = 0.087×10^{11} counts for a point source contained in a 5″ × 5″ aperture (or 0.174×10^{11} total counts). This ECF is appropriate for thermal emission from warm gas ($kT \sim 0.5$–1.0 keV) seen through the Galactic H I column density of 2.1×10^{21} cm^{-2}. The fluxes correspond to unattenuated fluxes (i.e., as measured if N[H I] = 0). Col. (4): The luminosities (in units of 10^{38} ergs s^{-1}) corresponding to the fluxes in col. (3) for our adopted distance of 2.2 Mpc for NGC 1569. Col. (5): The rough size of the X-ray components. See text.

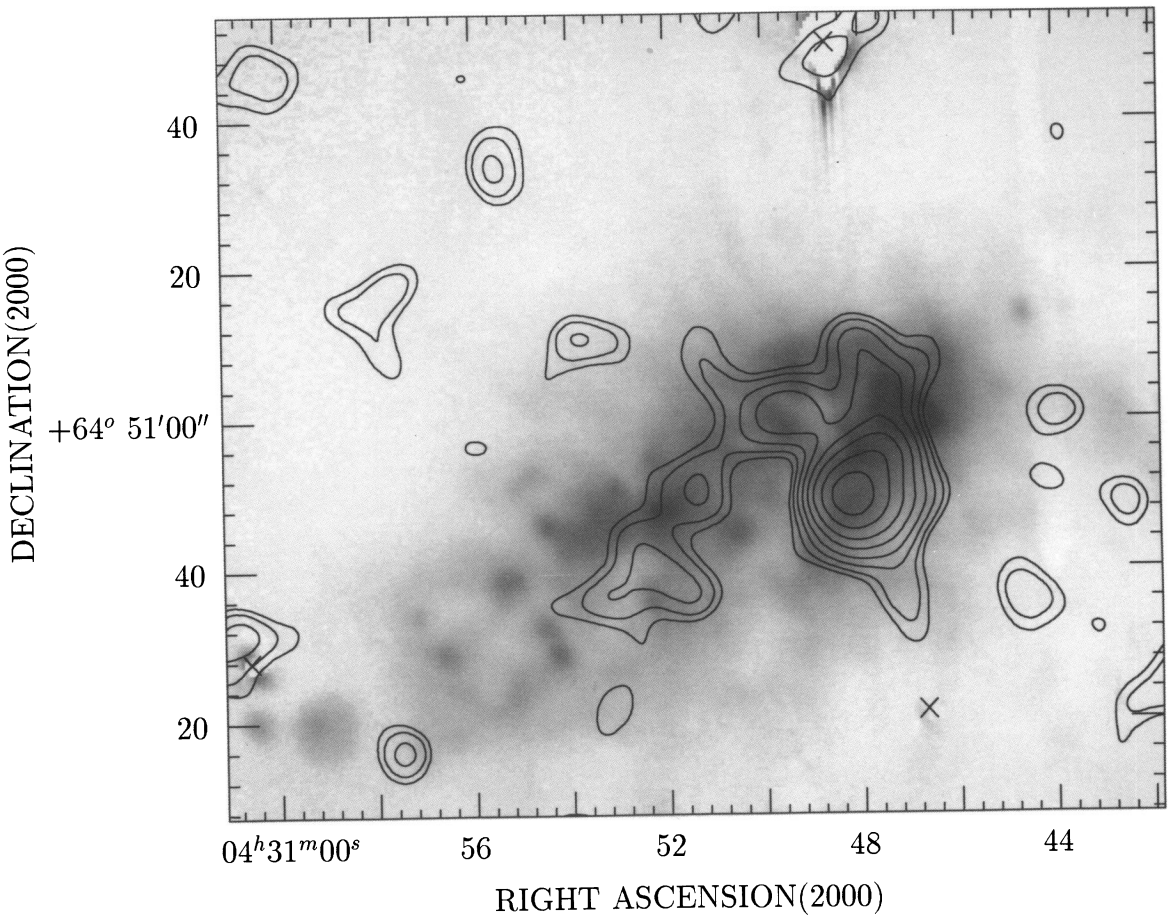

FIG. 1*b*

PLATE 2

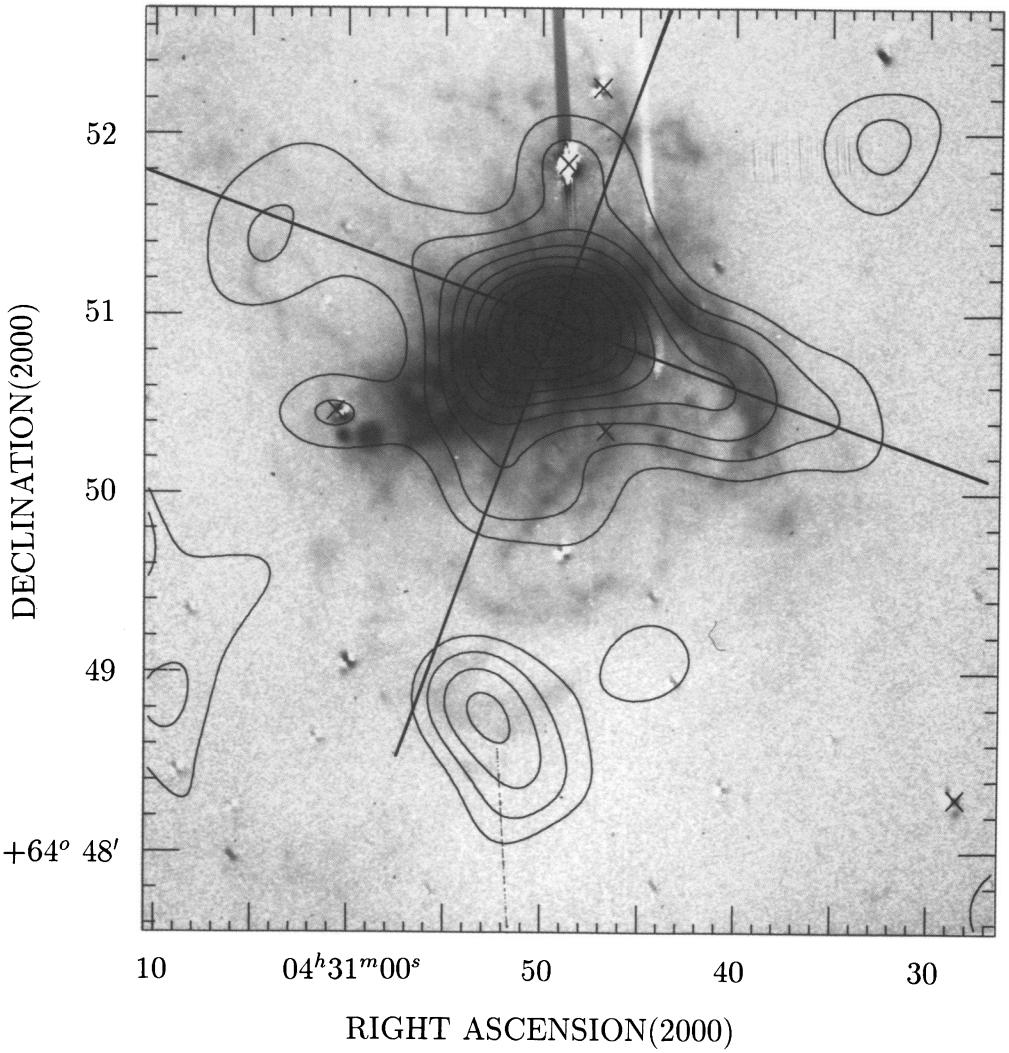

FIG. 1c

nosity in the 0.1–2.4 keV band is then 4.9×10^{38} ergs s^{-1} for the warm thermal model. This will increase to 5.7×10^{38} ergs s^{-1} if we include the detached "blob" of X-ray emission about 2′ south of the galaxy (see below).

The above fluxes can be compared to the flux of $1.9 \pm 0.2 \times 10^{-12}$ ergs cm^{-2} s^{-1} measured with the IPC onboard the *Einstein Observatory* in the 0.2–4 keV band, assuming a 5 keV thermal model (Fabbiano et al. 1992). Note, however, that this IPC flux contains a contribution from an X-ray–bright star located about 3′ to the east-southeast of NGC 1569, which is detected with 118 ± 12 total counts in our HRI image (i.e., 70% as many counts as NGC 1569 itself).

In an azimuthally averaged plot of the X-ray radial surface brightness profile, the X-ray emission from NGC 1569 can be detected out to a radius of about 1.′6 = 1.0 kpc at an isophotal level of 0.009 counts $pixel^{-1}$ ($\sim 2.0 \times 10^{-17}$ ergs cm^{-2} s^{-1} $arcsec^{-2}$) above the background. This is similar to the overall size of the Hα filament system (Waller 1991; Hunter et al. 1993), the standard optical isophotal radius for the galaxy (de Vaucouleurs et al. 1991), the size of the nonthermal radio continuum halo (Israel & de Bruyn 1988), and the overall extent of the H I (Israel & van Driel 1990). The "half-light radius" for the X-ray source is 30″ = 320 pc, which is quite similar to the half-light radii of both the Hα emission (24″ = 260 pc) and the blue light (26″ = 280 pc). We have measured the half-light radius for the Hα emission using an azimuthally averaged growth curve centered on the midpoint between super starclusters A and B. We summarize all the relevant size scales for NGC 1569 in Table 3.

In Figures 1*a*–1*b* the structure of the bright core of the X-ray emission can be discerned. The core is resolved into a lumpy ridge that extends about 50″ (550 pc) roughly along the galaxy major axis. A bright knot is visible south of the west-northwest end of the ridge. This knot is resolved in our full-resolution image (Fig. 1*a*) into a pair of point sources separated by about 6.″5 (70 pc) in PA $\sim -40°$ (hereafter sources 1 and 2). Sources 1 and 2 have fluxes of about $1.6 \pm 0.4 \times 10^{-13}$ and $8 \pm 3 \times 10^{-14}$ ergs cm^{-2} s^{-1}, respectively, corresponding to luminosities of about 9×10^{37} and 4.5×10^{37} ergs s^{-1}. These point sources then comprise about 30% of the total X-ray flux. Excluding these point sources, the rest of the bright ridge has a flux of about $1.7 \pm 0.4 \times 10^{-13}$ ergs cm^{-2} s^{-1}, or a luminosity of 1.0×10^{38} ergs s^{-1}.

As Figure 1*b* shows, there is a general (but not a detailed) correspondence between the morphology and size of the X-ray and Hα emission in the starburst region. Waller (1991) has measured the Hα fluxes for 12 giant H II regions within the bright central Hα complex in NGC 1569. The three brightest H II regions are numbers 2, 3, and 7 in his notation. H II regions 2 and 3 may be associated with the brightest X-ray emission in our high-resolution image (they are located about 13″ and 6″ to the north-northwest respectively of the centroid of our sources 1 and 2). This region also corresponds to the peak in the far-IR surface brightness in NGC 1569 (Hunter et al. 1989). H II region 7 is about 9″ north of a fainter X-ray knot at the southeast end of the X-ray ridge. The super starclusters A and B (see O'Connell et al. 1994) are about 6″ northeast of X-ray sources 1 and 2, respectively. Note that these offsets are significantly larger than the 2″ positional accuracy of the HRI image relative to the optical (see § 2.1 above). We see no significant X-ray emission associated with the Wolf-Rayet star and its ring nebula that were recently discovered by Drissen & Roy (1994).

We conclude that sources 1 and 2 are either X-ray binaries or unusually bright supernova remnants. They are pointlike at the 5″ resolution of the HRI, and each has an X-ray luminosity well within the range of X-ray binary sources (see Nagase 1989). They could also be X-ray-luminous supernova remnants like N132D and N63A in the LMC which have similar X-ray luminosities (Long, Helfand, & Grabelsky 1981). Note that they are considerably less luminous than the members of the peculiar class of superpowerful old supernova and/or young supernova remnants like SN 1978K, SN 1986J, and the remnants in NGC 4449 and NGC 6946 (see Schlegel 1994, and references therein). The X-ray ridge is most likely produced by thermal emission from diffuse hot gas, although we cannot rule out the possibility that it is instead a superposition of many (five or more) weak point sources, such as X-ray binaries or supernova remnants. Since an average O star has an X-ray luminosity of only 10^{32}–10^{33} ergs s^{-1} (see Vaiana 1990), the X-ray ridge is at least an order of magnitude too luminous to be produced by the ensemble of 3000–10,000 O stars estimated to be present in NGC 1569 (see § 4.2.1 below).

The remaining half of the X-ray emission from NGC 1569 is diffuse and cannot be directly discerned in the full-resolution or high-resolution images. As our low-resolution image in Figure 1*c* clearly shows, this diffuse emission consists of a low surface brightness halo with a maximum extent of about 3.′8 (2.4 kpc) in the east-northeast to west-southwest direction. Apart from the bright central sources discussed above, there are several spurs of X-ray emission visible in Figure 1*c*. The brightest spur extends about 1.′8 (1.2 kpc) to the west-southwest, and a fainter counterpart of similar extent can be seen on the opposite side (east-northeast). The third spur extends about 1.′2 (750 pc) to the south-southeast. A fourth feature located about 1′ to the north is possibly confused by weak X-ray emission from an optically bright foreground Galactic star. There is also a detached "blob" of X-ray emission about 2.′3 to the south-southeast of the galaxy which may possibly be associated with NGC 1569. This feature has a flux of $1.2 \pm 0.4 \times 10^{-13}$ ergs cm^{-2} s^{-1} ($L \sim 7 \times 10^{37}$ ergs s^{-1} if associated with NGC 1569). Note that the faint X-ray contours at the lower left edge of Figure 1*c* are the wings of the PSF of the X-ray bright star located about 3′ to the east-southeast of NGC 1569 (just off the edge of the displayed field).

TABLE 3

X-RAY, OPTICAL, AND RADIO SIZE SCALES IN NGC 1569

Units (1)	D_X (2)	$r_{e,X}$ (3)	D_B (4)	$r_{e,B}$ (5)	$D_{H\alpha}$ (6)	$r_{e,H\alpha}$ (7)	$D_{H\,I}$ (8)	D_{sync} (9)
arcmin.....	4.0	0.50	3.6	0.43	5.5	0.4	7.0	3.5
kpc	2.6	0.32	2.3	0.28	3.5	0.26	4.5	2.2

NOTES.—Col. (1): Units appropriate to the entries on each row; col. (2): Diameter of the X-ray halo at our limiting surface brightness. This includes the southern "blob" (see text). For our adopted ECF (see Table 2 and text) the limiting surface brightness corresponds to 2.3×10^{-17} ergs cm^{-2} s^{-1} $arcsec^{-2}$ for a diffuse source; col. (3): The X-ray "effective radius" (radius within which half the total counts are contained); col. (4): The optical diameter of the galaxy (major axis) at a limiting surface brightness of 25 *B* magnitudes per square arcsec (after correction for Galactic extinction). Taken from de Vaucouleurs et al. 1991; col. (5): The optical (*B*) effective radius from de Vaucouleurs et al. 1991; col. (6): The diameter of the Hα filament system at a limiting Hα surface brightness of about 10^{-15} ergs cm^{-2} s^{-1} $arcsec^{-2}$, taken from Hunter, Hawley, & Gallagher 1993; col. (7): The Hα effective (half-light) radius, measured by us from the image published in Hunter, Hawley, & Gallagher 1993; col. (8): The H I diameter (major axis) at an H I column density of 1.8×10^{20} cm^{-2} (Israel & van Driel 1990); col. (9): The diameter of the radio synchrotron halo measured at a limiting surface brightness at 1.415 GHz of 1.5 mJy per 24″ × 27″ synthesized beam (Israel & de Bruyn 1988).

Optical continuum images show NGC 1569 to be a rather flat system ($a/b \sim 2$) with a major axis in a position angle of about 120°. Thus, the diffuse X-ray emission lies preferentially along the optical minor axis (as does the well-known Hα filament system). Indeed, there is a good morphological correspondence between the X-ray and Hα emitting material. The Hα filaments appear to define several large-scale nested loops or bubble-like structures. That is, the filaments have quasi-radial orientations in the inner region and arclike circumferential orientations at their outer extremities (see Fig. 1*c* and also Waller 1991; Hunter et al. 1993). The brightest such Hα loop or filament extends out about 1.'3 to the west-southwest (coinciding with the brightest X-ray spur). The second brightest Hα structure extends about 1.'5 to the north, where our X-ray image is possibly confused by a Galactic star. An Hα loop or bubble is visible in the region of the south-southeast X-ray spur, and an outer Hα loop or bubble is coincident with the detached "blob" of diffuse X-ray emission some 2.'3 to the south-southeast. Finally, a system of faint Hα filaments extend out 2.'5 to the west-northwest near the corresponding X-ray spur.

The close morphological relationship between the X-ray halo and the Hα filaments strongly suggests that the emission from the former is produced by thermal emission from diffuse hot gas. We have therefore derived the basic physical properties of the X-ray halo source under the assumption that it is indeed produced by hot gas (Table 4). We will consider this idea in detail in § 4.3.1 below. The X-ray halo also resembles the nonthermal radio halo mapped by Israel & de Bruyn (1988). Thus, inverse Compton emission from the relativistic electrons responsible for the nonthermal radio halo could in principle contribute to the X-ray halo. This is not likely to be the dominant emission mechanism, however, as we will discuss in more detail in § 4.3.2 below.

It is also instructive to compare the morphology of the X-ray halo and Hα filament system to that of the H I map by Israel & van Driel (1990), since the H I comprises the bulk of the ISM mass in NGC 1569. Their 24″ resolution map shows that the size and orientation of the H I is rather similar to the starlight in NGC 1569: (roughly 6′ × 3′ ∼ 4 × 2 kpc, with a major axis in PA ∼ 120°). There is also a "spur" of H I which extends to about 4′ ∼ 2.6 kpc south-southeast of the galaxy. This spur lies in the same direction as (but extends beyond) the faint Hα arcs and detached X-ray blob visible in Figure 1*c*. The X-ray blob is located at a local minimum in the H I column density in the spur. This correspondence makes it more likely that the faint X-ray blob is in fact physically associated with NGC 1569. The entire X-ray halo and Hα filament system therefore lies within the H I distribution of NGC 1569, at least in projection (which is an important caveat). This suggests that the X-ray and Hα emission may arise as the result of the interaction between the kinetic energy supplied by the starburst and the relatively dense and cool ambient gas in the ISM of NGC 1569 (as we will discuss in detail in § 4.)

3. OPTICAL SPECTROSCOPY

3.1. *Observations and Data Analysis*

The optical spectroscopic data for NGC 1569 were obtained on the night of 1994 January 12, using the Ritchey-Chrétien spectrograph on the 4 m Mayall telescope at the Kitt Peak National Observatory. We used the KPC-24 grating (860 line mm^{-1}) in second-order with a GG495 filter to block the third order. With the Tektronix 2048 CCD (T2KB) as a detector, the resulting pixel scale was 0.''69 × 0.52 Å. The slit used was 2.''0 wide by 310″ long, and the spatial resolution as measured using bright stars was about 3 pixels (2.''1 FWHM). The spectrum covered the wavelength range from 5780 to 6835 Å with a resolution FWHM of about 1.25 Å at Hα (57 km s^{-1}), based on measurements of night-sky lines. Two exposures of 1800 s duration were obtained in each of two position angles (70° and 160°), chosen to pass through the most prominent X-ray plumes seen in our HRI image. The spectrograph slit was centered on the region of peak surface brightness as judged in the image seen through the red-sensitive acquisition camera on the telescope. This corresponds to the "super star cluster A,"

TABLE 4

PHYSICAL CONDITIONS AND ENERGETICS OF THE HALO

kT (1)	L_x (2)	EI (3)	$\langle n_x \rangle$ (4)	P_x (5)	P_{rad} (6)	P_{opt} (7)	M_x (8)	M_{opt} (9)	E_x (10)	E_{rad} (11)	KE_{opt} (12)	t_{cool} (13)
0.5.....	2.6	9.3	$8.7f^{-1/2}$	$1.3f^{-1/2}$	$\simeq 1$	$\lesssim 28$	$9.2f^{1/2}$	$\gtrsim 3$; 10	$2.7f^{1/2}$	4.4	$\gtrsim 0.03$; 0.1	$0.35f^{1/2}$
1.0.....	2.5	6.4	$6.7f^{-1/2}$	$2.2f^{-1/2}$	$\simeq 1$	$\lesssim 28$	$7.6f^{1/2}$	$\gtrsim 3$; 10	$4.5f^{1/2}$	4.4	$\gtrsim 0.03$; 0.1	$1.0f^{1/2}$
5.0.....	3.5	34	$15f^{-1/2}$	$25f^{-1/2}$	$\simeq 1$	$\lesssim 28$	$18f^{1/2}$	$\gtrsim 3$; 10	$51f^{1/2}$	4.4	$\gtrsim 0.03$; 0.1	$2.1f^{1/2}$

NOTES.—Col. (1): The temperature (kT in keV) assumed for the other entries on the same line; col. (2): The luminosity in the 0.1–2.4 keV band (in units of 10^{38} ergs s^{-1}). This pertains to the X-ray halo excluding the detached southern "blob" (see Table 2 and text); col. (3): The emission integral $\int n_x^2\, dV$ (in units of 10^{60} cm^{-3}) implied by the luminosity in col. (2); col. (4): The mean density of the X-ray–emitting gas in units of 10^{-3} cm^{-3}. This is obtained from col. (3) assuming a total source volume of 1.3×10^{65} cm^3 (equivalent to a sphere with a radius of 1 kpc). The emitting gas is assumed to have a volume-filling factor f within the source volume; col. (5): The pressure in the X-ray–emitting gas (in units of 10^{-11} dyn cm^{-2}) implied by the density in col. (4) and the temperature in col. (1); col. (6): The pressure estimated in the radio synchrotron plasma in the halo assuming minimum energy conditions. See Israel & de Bruyn 1988 for details. The units are 10^{-11} dyn cm^{-2}; col. (7): An upper limit to the pressure in the optical emission-line gas in the halo based on the measured upper limit to the electron density (see text for details). The units are 10^{-11} dyn cm^{-2}; col. (8): The mass of the X-ray–emitting gas (in units of 10^5 $M_\odot$) implied by the density in col. (4) and the assumed source volume and filling factor (f); col. (9): The mass of the optical emission-line filaments (in units of 10^5 $M_\odot$). This estimate pertains only to the high-velocity gas, which provides about 25% of the total Hα luminosity. It assumes Case B recombination and a temperature of 10^4 K (see Osterbrock 1989). The lower limit corresponds to the upper limit measured for the electron density. The second value pertains if the optical emission-line filaments are at the pressure predicted by eq. (4) in the text; col. (10): The thermal energy content of the X-ray–emitting gas (in units of 10^{54} ergs), based on the mass in col. (6) and the temperature in col. (1); col. (11): The total energy in the radio synchrotron plasma, assuming minimum energy conditions (see Israel & de Bruyn 1988 for details). The units are 10^{54} ergs; col. (12): The total kinetic energy of the high-velocity optical emission-line filaments. The mass comes from col. (9), and the assumed velocity is 100 km s^{-1}. The units are 10^{54} ergs; col. (13): The radiative cooling time for the gas (in Gyr), based on the density in col. (4), the temperature in col. (1), and the radiative cooling curve of Sutherland 1993.

which is the brighter of the super star clusters in NGC 1569—see O'Connell et al. (1994). An 1800 s exposure of the night sky was obtained in position angle 160° immediately after the galaxy spectra.

The data were reduced in the standard way in IRAF. A DC level was subtracted from all frames using the overscan columns on the CCD. A two-dimensional bias frame was formed from the median of a series of individual bias frames (frames with zero integration time), and this image was subtracted from all the other frames. The data were flat-fielded using a frame formed from a series of exposures of a dome screen illuminated by a quartz lamp. HeNeAr arc lamp exposures taken after each series of galaxy exposures at a given position angle were used to determine the full dispersion solution along the slit for each spectrum, and this solution was used to geometrically rectify and wavelength-calibrate the spectra. The zero points of these solutions were verified using measurements of bright night-sky lines in the galaxy spectra. The spectra were flux-calibrated using observations of Hiltner 102, observed with the slit jaws opened to 10″.

For the data in P.A. = 70°, the sky was subtracted interactively using the IRAF task BACKGROUND to fit a low-order polynomial to those regions of the sky along the slit that were free of conspicuous Hα emission. For the data in P.A. = 160°, the exposure of the blank sky was smoothed by 10 pixels along the slit direction to improve its signal-to-noise ratio, and then subtracted from the galaxy spectrum. Small residuals were then further removed using BACKGROUND (as for P.A. = 70°). Residual uncertainties in the sky subtraction seriously affect our measurements of the rather weak [O I] λ6300 nebular line in NGC 1569, since this line is the strongest night-sky line, and since the emission-line gas in NGC 1569 had a geocentric velocity range from about +100 to −200 km s^{-1}. Thus, we were able only to measure this line in the central region of the galaxy where it reached its peak surface brightness. We also produced a pair of spectra from which the galaxy continuum (starlight) was subtracted. To do so, we used the task BACKGROUND to fit a low-order cubic spline along the dispersion direction on a row-by-row basis using only the pixels that were not affected by significant emission or absorption lines.

For analysis, the spectra were binned in the spatial direction by three pixels ∼2.″1. For each binned spectum the IRAF task SPLOT was used interactively to determine the flux (zeroth moment), flux-weighted centroid (first moment), and equivalent width for the He I λ5876, [O I] λ6300, Hα, [N II] λ6584, and [S II] λλ6717, 6731 emission lines. The emission-line profiles are strongly non-Gaussian at most positions. The strong Hα emission-line profile was therefore fitted with multiple Gaussians (either two or three components as warranted). At many locations, the emission-line profile is double-peaked or triple-peaked with clear minima in the intensity between these peaks. At many other locations, the profile is not clearly multiply peaked but is decidedly non-Gaussian with a narrow "core" and broad asymmetrically located "wings" or "shoulders." We have also fitted such profiles with two or three Gaussian components as warranted, although the evidence for multiple independent kinematic components is not as unambiguous as for the profiles with clear multiple intensity peaks. For each Gaussian component, a line width was determined, and these were corrected for instrumental broadening, assuming that the measured width was the sum in quadrature of the intrinsic line width and the instrumental resolution.

3.2. *Results*

3.2.1. *Kinematics*

The long-slit spectra in the region of the Hα and [N II] λλ6548, 6584 emission lines are shown in gray-scale form in Figures 2*a*–2*b* (Plates 3–4), and a contour representation of the Hα emission alone in both positions angles is shown in Figure 3. In Figures 4*a*–4*b* we show the results of the multicomponent fitting of the Hα emission-line profiles described in § 3.1 above. The most striking features are the large structures with fragmented, incomplete–oval-shaped morphologies in position-velocity space. These are reminiscent of the classical behavior of the expanding shells of planetary nebulae (see Fig. 6.6 in Osterbrock 1989). We will follow convention and henceforth denote these spectroscopic features as "Doppler ellipses."

Perhaps the clearest example of a Doppler ellipse is the structure that extends between radii of 10″–55″ (110 pc) to the west-southwest of super star cluster A in P.A. 70. The structure is most clearly seen in the [N II] λ6584 emission line in Figure 2*a*. This Doppler ellipse corresponds to the interior of the brightest Hα loop seen in Figure 1*c*. The velocity separation of the two kinematic components at the center of the Doppler ellipse (located ∼25″–30″ west-southwest of super star cluster A) is about 160 km s^{-1}. We note that the spectra discussed by TOS did not cover the central region of this Doppler ellipse (their measurements to the west-southwest were made only out to about 17″ from super star cluster A in P.A. 70).

Another relatively clear Doppler ellipse can be seen in our data in the region extending from 30″ to 75″ (320–800 pc) north-northwest of the super star cluster A in P.A. 160 (Figs. 2*b*, 3, and 4*b*). The maximum velocity separation at the center of this Doppler ellipse is about 260 km s^{-1}. This entire kinematic structure corresponds well to an Hα loop just to the west of the bright Galactic star in Figure 1*c*. The structure lies outside (to the north of) the region mapped by TOS.

To the south-southeast in P.A. 160, the kinematics of the gas are more complex (Figs. 2*b*, 3, and 4*b*). The region extending out to about 2.′4 (∼1.5 kpc) from the galaxy center appears to consist of a nested set of fragmented, incomplete Doppler ellipses. Typical velocity separations between the red- and blueshifted kinematic components are 150–250 km s^{-1} in this region. Likewise, the Hα morphology of this region (Fig. 1*c*) shows a series of circumferentially oriented filaments or arcs that appear to define the walls of fragmented bubbles. The data presented by TOS cover only the region within 40″ of the super star cluster A to the south-southeast, and so miss these structures.

Even the very faint filamentary gas to the east-northeast in P.A. 70 appears to define a very fragmentary, partial Doppler ellipse in the region located about 1.′0–1.′8 (0.6–1.2 kpc) from super star cluster A in our P.A. 70 spectrum. The velocity separation of the kinematic components here is about 150 km s^{-1}. This region was missed by TOS, whose data extend only out about 0.′6 in this direction.

The decomposition of the Hα emission-line profiles into multiple components strongly suggests the presence of two kinematically distinct subsystems in NGC 1569. These are a relatively bright and centrally located "quiescent system" and a fainter and more extended "high-velocity system." The presence of these two kinematic systems has also been emphasized by TOS, although (as noted above) their slit coverage missed the most dramatic examples of high-velocity gas seen in our data (they primarily mapped the high surface brightness

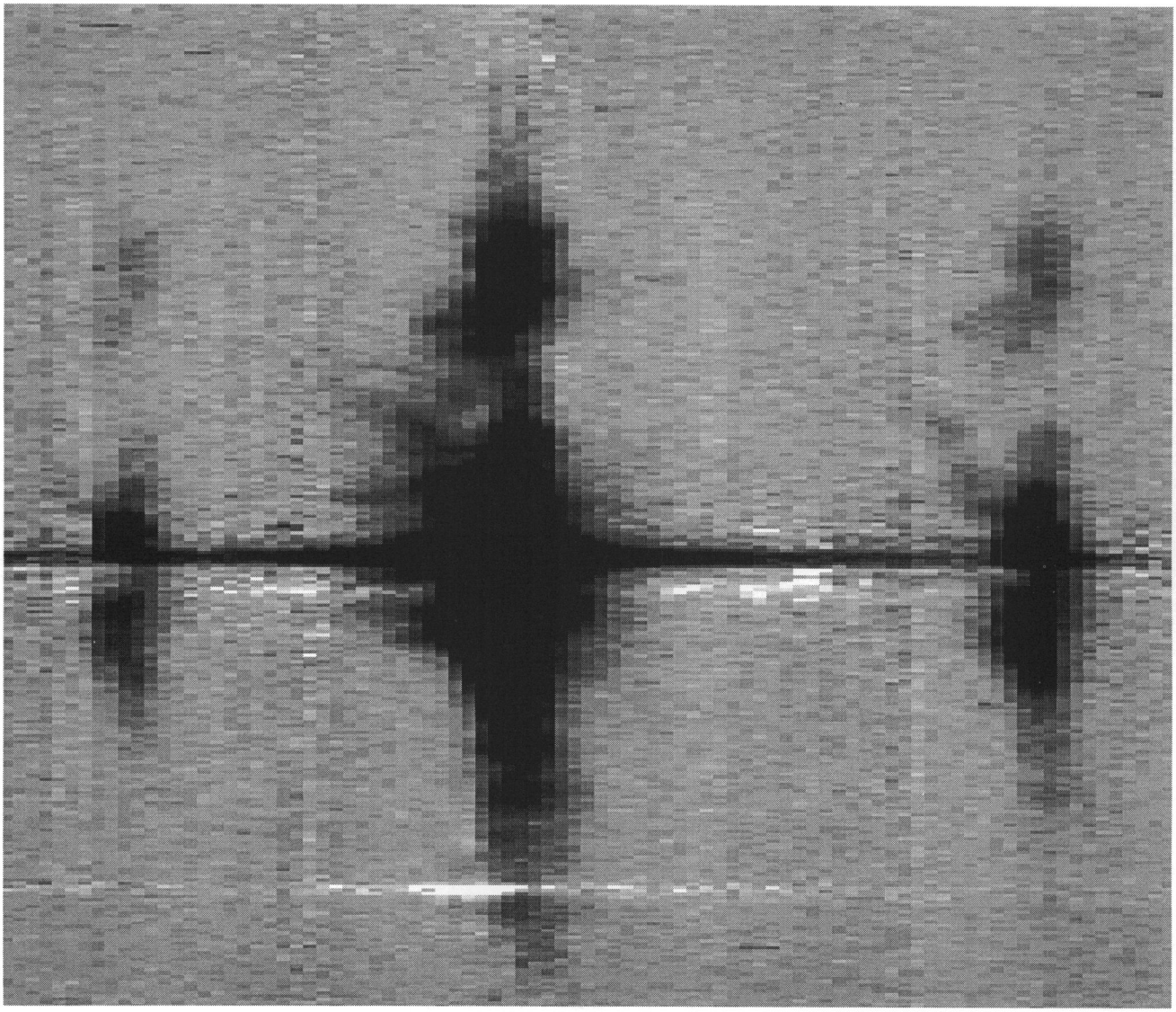

FIG. 2*a*

FIG. 2.—(*a*) A gray-scale display of our KPNO 4 m long-slit spectrum (P.A. = 70°) of (from left to right) the [N II] λ6548, Hα, and [N II] λ6584 emission-lines. The galaxy continuum has been subtracted from this image leaving only the emission lines (see text). The region displayed is ~3.'5 in size, with west-southwest to the top and east-northeast to the bottom. Note the fragmented Doppler ellipse in the region 10″ to 55″ to the west-southwest of the center (seen most clearly in the [N II] λ6584 line). Several spatially compact regions with broad emission lines can be seen in the Hα line. (*b*) Same as (*a*), but in P.A. = 160°. The region displayed is ~4.'0 in size, with north-northwest to the top and south-southeast to the bottom. Note the Doppler ellipse in the region 30 to 75″ north-northwest of the galaxy center (seen in Hα). The entire region extending out some 2.'4 to the south-southeast appears to consist of a nested set of fragmented, incomplete Doppler ellipses. Several compact regions with broad emission lines can be seen in the Hα line.

PLATE 4

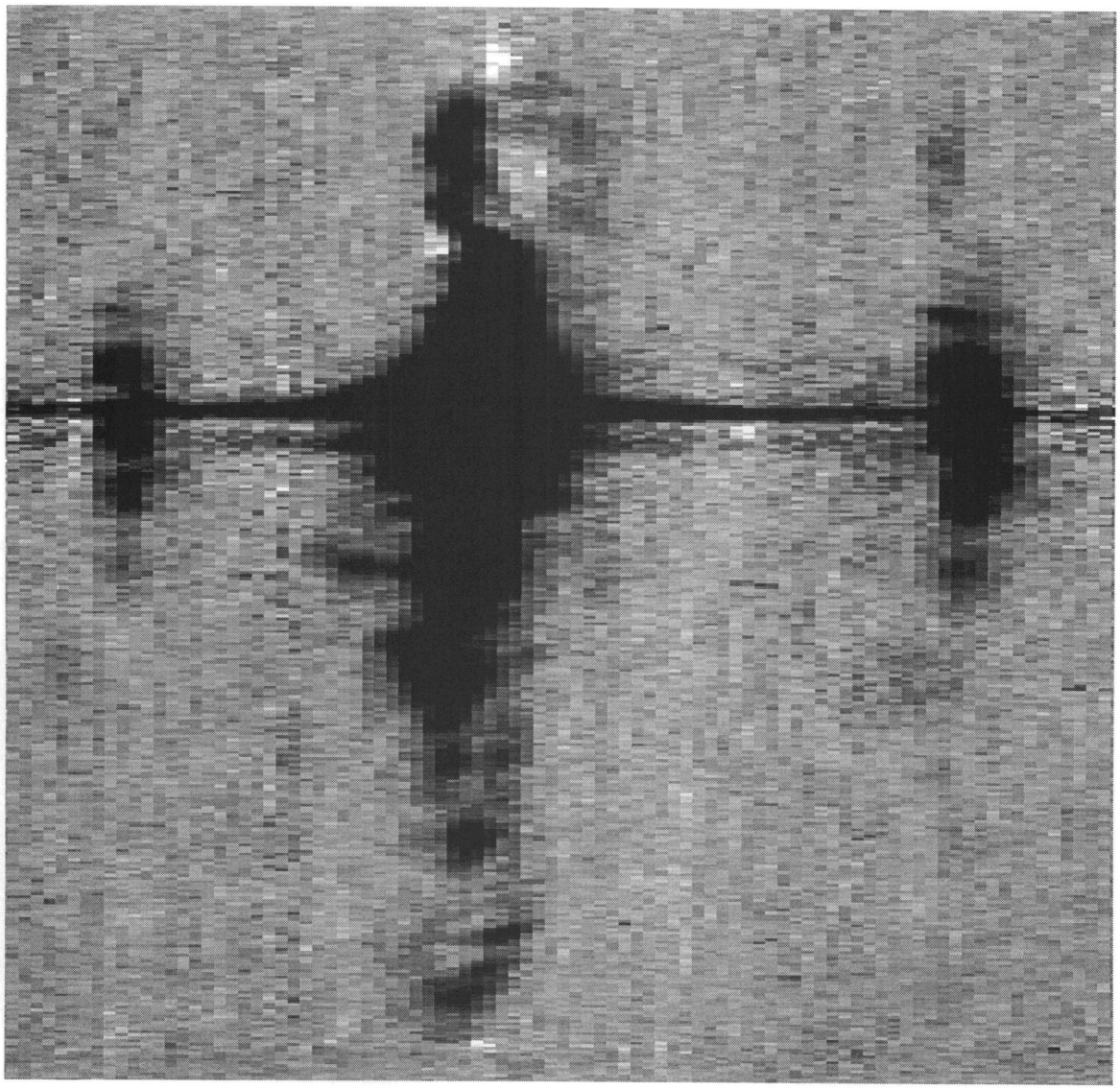

FIG. 2*b*

HECKMAN et al. (see 448, 104)

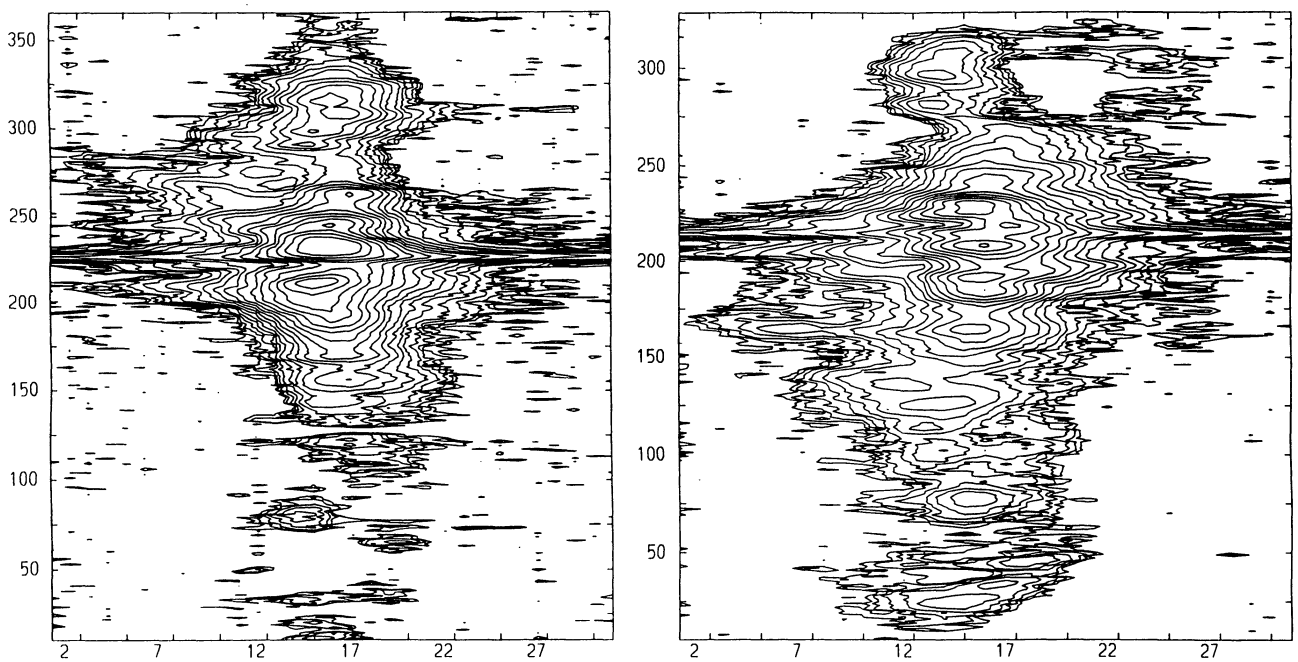

FIG. 3.—*Left panel*: Contour plot of the Hα line emission in our long-slit data in P.A. = 70°. The galaxy continuum has been subtracted from this image leaving only the emission lines (see text). The orientation is the same as in Fig. 2*a*. The coordinates are given in pixel numbers. One pixel covers 0.52 Å (24 km s^{-1}) along the horizontal axis and 0″.69 (7.4 pc) along the vertical axis. The total size of the displayed image is then 16 Å (740 km s^{-1}) by 259″ (2.8 kpc). The galaxy center (super star cluster A) is located at pixel 227 along the vertical axis. The lowest contour is at a level of 4.4×10^{-18} ergs cm^{-2} s^{-1} $arcsec^{-2}$ $Å^{-1}$, and each successive contour represents an increase in surface brightness by 0.2 dex (roughly a factor 1.58). *Right panel*: The same, but in P.A. = 160°. The orientation is the same as in Fig. 2*b*, and the total size of the image displayed is 16 Å (740 km s^{-1}) by 230″ (2.5 kpc). The location of the super star cluster A is at pixel 215 along the vertical axis.

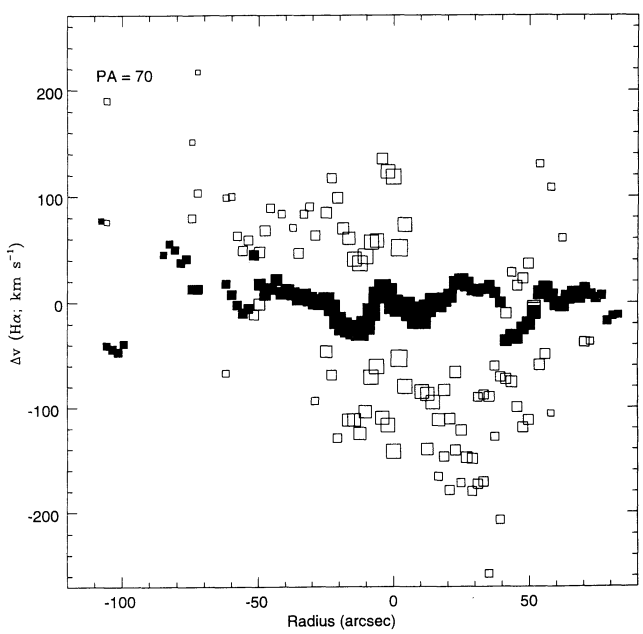

FIG. 4*a*

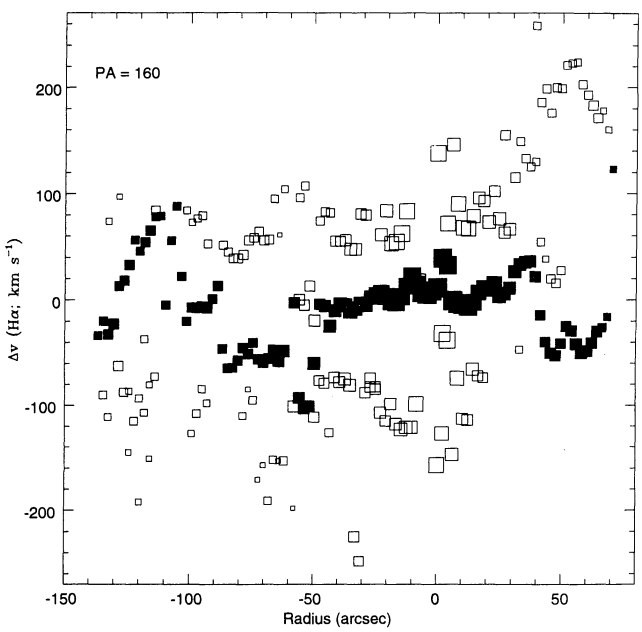

FIG. 4*b*

FIG. 4.—(*a*) Representation of the velocity field as defined by the Hα emission line in our spectrum along P.A. = 70°. In each 2″.1 spatial increment, the Hα profile has been fitted with one to three Gaussian subcomponents as warranted (see text). The radial velocity of each component is plotted relative to our adopted v_{sys} of −68 km s^{-1} (heliocentric) on the vertical axis. The brightest component at each location is indicated by the solid box and the fainter component(s)—if present—by one or two hollow boxes. The size of the box is proportional to the log of the flux of the component it represents. The spatial location of each box is indicated on the horizontal axis relative to the pixel with the peak surface brightness in the continuum (super star cluster A). East-northeast is to the left and west-southwest is to the right. (*b*) The same as 4*a*, but in P.A. = 160° with south-southeast to the left and north-northwest to the right.

material in or near the galaxy disk but did not map the fainter outlying filaments). The quiescent system is characterized by radial velocities within about 30 km s^{-1} of v_{sys} (the systemic velocity) and line widths of typically 30–90 km s^{-1} (FWHM). In contrast, the gas in the high-velocity system extends to radial velocities of over 200 km s^{-1} relative to v_{sys}, and has line widths that range up to 150 km s^{-1}. Note that these widths refer to the Gaussians used to fit the individual components in the emission-line profile (after correction for instrumental line broadening—see § 3.1).

Consider first the data in P.A. 160 (Figs. 2*b*, 3, 4*b*). Within ±30″ (320 pc) of the center (super star cluster A), the brightest component of the emission-line profile is at all locations within about 30 km s^{-1} of the galaxy systemic velocity. In the same region, two fainter kinematic components are also present with velocities of roughly +100 and −100 km s^{-1} relative to v_{sys}. These appear in the form of relatively broad wings on the Hα emission-line profiles within this region (see Fig. 3*b*). The high-velocity system extends out considerably farther than the quiescent system in P.A. 160, forming the Doppler ellipses discussed above.

In P.A. 70 (Figs. 2*a*, 3, 4*a*), the bright quiescent system extends about 1′ (600–700 pc) on either side of the galaxy center. In this position angle, the faint high-velocity gas shows a shear of roughly 200–250 km s^{-1} from the redshifted gas to the east-northeast to the blueshifted gas to the west-southwest. The sense of the velocity shear agrees with that found by de Vaucouleurs (1981) in his Fabry-Perot data, but the amplitude we find is about a factor of 2 larger (since we ignore the bright emission from the quiescent system which "dilutes" the shear seen in the fainter high-velocity system). The high-velocity blueshifted gas comprises the material located 20″–55″ to the west-southwest (i.e., the blueshifted part of the Doppler ellipse described above), and two regions each extending out about 17″ to the east-northeast and west-southwest of the super star cluster A. To the east-northeast, the high-velocity redshifted gas can be seen out to a radius of about 50″ in the form of a redward "wing" on the Hα emission-line profile (see Fig. 3).

A comparison of Figure 4 to Figure 1 implies that the quiescent system is most likely the high surface brightness material located in or very near the starburst region of the galaxy. The high-velocity system would then correspond to the fainter and more extended Hα filaments (which will also be seen in projection in the central region dominated by the quiescent system). Summing the fluxes of the individual components in our multicomponent Hα emission-line profile fitting, we find that about 75% ± 10% of the Hα emission comes from the quiescent component and 25 ± 10% from the high-velocity component along P.A. 70 and P.A. 160.

As shown in Figure 5, the Hα emission-line profile in the central region (a box roughly 2″.0 in size centered on super star cluster A) of both our spectra shows weak but exceptionally broad wings which have a full width at zero intensity of at least 30 Å, and possibly 50 Å (~1400–2300 km s^{-1}). The flux of this broad component is about 2.5×10^{-14} ergs cm^{-2} s^{-1} (about 30% of the total Hα flux in the same aperture). The implied Hα luminosity of the broad component is $\sim 6 \times 10^{37}$ ergs s^{-1}. Similar very broad wings on optical emission-line profiles have been recently discovered in the central regions of several other dwarf starburst galaxies (MHWS; Meurer 1989; Roy et al.

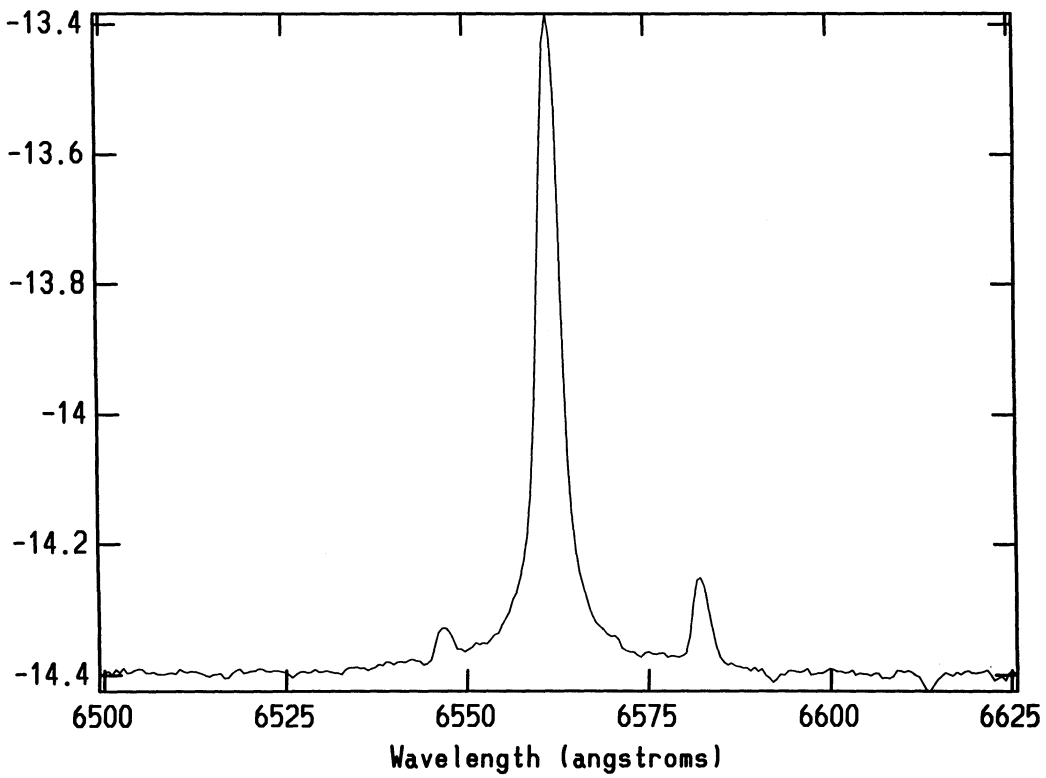

FIG. 5.—The Hα emission-line profile in a 2″.0 × 2″.1 region centered on super star cluster A (average of data in both position angles). The vertical axis plots the log of the flux density (in units of ergs cm^{-2} s^{-1} $Å^{-1}$), in order to more clearly show the faint but very broad "wings" on the Hα profile. These wings extend over at least 30 Å (1400 km s^{-1}) and possibly as much as 50 Å (2300 km s^{-1}). The narrow [N II] λλ6548, 6584 lines are also evident.

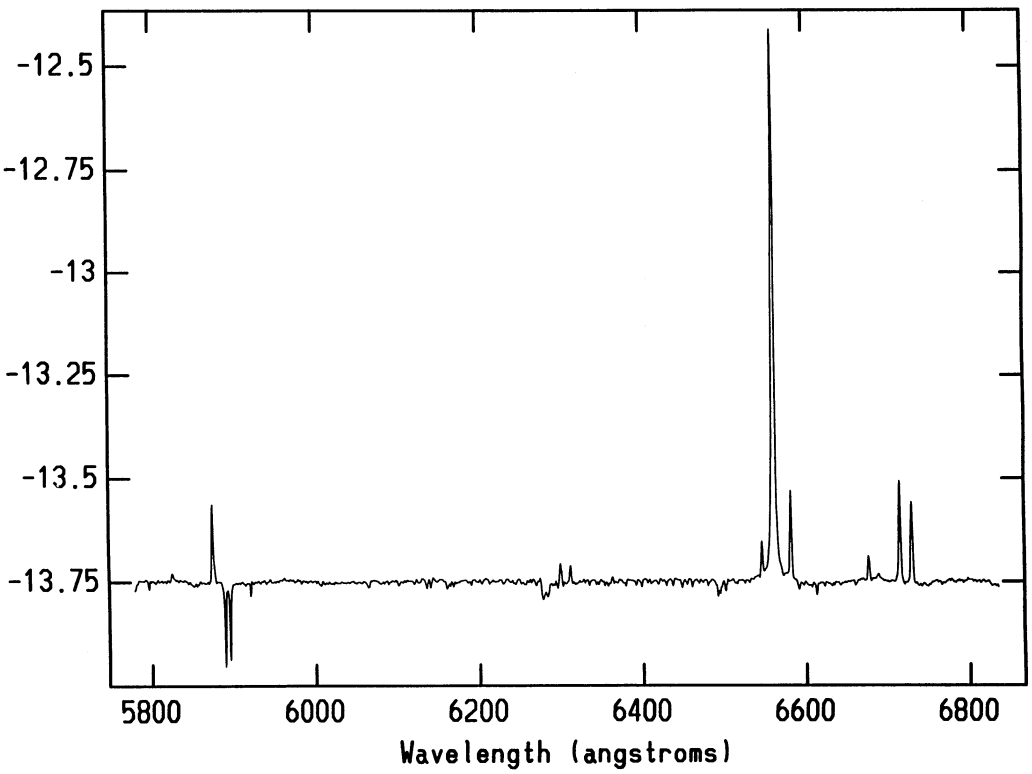

Fig. 6*a*

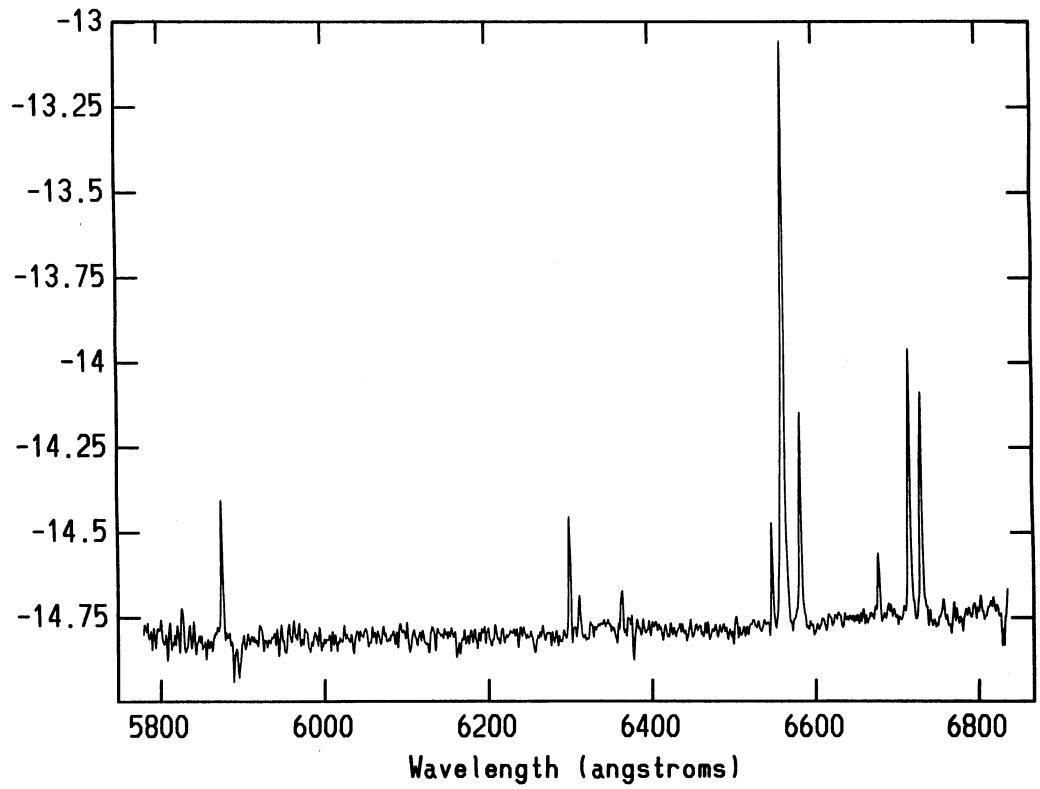

Fig. 6*b*

Fig. 6.—(*a*) The spectrum of the region within a radius of 5″ (53 pc) of the galaxy center (super star cluster A), summed over both position angles. The vertical axis plots the log of the flux density (in units of ergs cm^{-2} s^{-1} $Å^{-1}$), in order to show the very bright Hα line as well as the many much weaker spectral features. These include the He I λ5876, [O I] λ6300, [S III] λ6312, [N II] λ6548, [N II] λ6584, He I λ6678, and [S II] λλ6717, 6731 nebular emission lines and the Na I λλ5890, 5896 absorption lines (interstellar, presumably Galactic foreground, the O_2 absorption feature at 6277 Å (telluric), an absorption feature at 6284 Å (presumably the "diffuse" interstellar band arising in the Galactic foreground), and a feature at about 6495 Å which is a blend of stellar photospheric Ca and Fe absorption lines. (*b*) The same as Fig. 6*a* but summed over the annular region located between radii of 20″–40″ from super star cluster A. Here the [O I] λ6363 emission line can also be clearly seen. Compared to Fig. 6*a*, note the much greater strengths of the low-ionization [O I], [N II], and [S II] emission lines relative to the Hα and He I recombination lines.

1991; Thuan et al. 1994). The nature of energy source for these "broad-line regions" is not clear in general (see Roy et al. 1991). In the case of NGC 1569, we may be observing a relatively young ($\lesssim 10^4$ yr) Balmer-dominated supernova remnant in super star cluster A (see Smith et al. 1991).

In addition to this feature, there are several other spatially compact regions of high-velocity gas in NGC 1569. In these cases the high-velocity gas extends to "only" about 300 km s^{-1} blueward of the galaxy systemic velocity. Prominent examples can be seen in Figures 2 and 3 located about 12″ (125 pc) to the west-southwest and 15″ (160 pc) east-northeast of the super star cluster A in P.A. 70, and 35″ (380 pc) south-southeast of the cluster in P.A. 160. These may also be associated with individual supernova remnants or may be part of the complex system of expanding bubbles and nested Doppler ellipses described above.

3.2.2. *Physical Conditions in the Gas*

We find strong radial gradients in the flux ratios of the [O I] λ6300/Hα, [N II] λ6584/Hα, and [S II] λλ6717, 6731/Hα emission lines along both slit positions (Figs. 6*a*, 6*b*, and 7). The three respective ratios in the central-most region (within a few arcsec of super star cluster A) are roughly 0.4%, 2.5%, and 5%, while typical respective values in the filaments are 1%–3%, 6%–10%, and 20%–30%. Extreme values extend up to 5%, 20%, and 50%, respectively. While the radial gradients in the line ratios are large, the ratios themselves in the outer filaments are not unusual, being rather similar to the typical values that Hunter & Gallagher (1990) find for low surface brightness "froth" in irregular galaxies ([S II]/Hα ~ 30%–50% and [N II]/Hα ~ 10%–25%). As we discuss below, the enhanced relative strengths of low-ionization emission lines in the filaments of NGC 1569 may reflect either a contribution by shocks to the ionization of the gas or a decrease in the ionization state caused by the geometrical dilution of the ionizing radiation from the starburst.

We have also measured the density-sensitive ratio of the [S II] λλ6717, 6731 lines. Densities in the central-most 15″ are roughly 200 ± 100 cm^{-3}, but everywhere else the gas is at or near the low-density limit for the [S II] doublet ratio ($n_e < 100$ cm^{-3}). Outside the central region, the implied gas pressure for a nominal temperature of 10^4 K is $P \sim 2n_e kT < 2.8 \times 10^{-10}$ dyn cm^{-2}. This upper limit to the pressure is consistent with the pressure deduced for the nonthermal radio halo ($\simeq 10^{-11}$ dyn cm^{-2}) by Israel & de Bruyn (1988), and with the estimated pressures in the X-ray halo (see Table 4).

Finally, we measure the He I λ5876/Hα flux ratio to have a value of about 0.03 throughout the galaxy (in the starburst and outer filaments—see Fig. 6). Adopting an extinction correction of 1.45 mag at Hα (Waller 1991) and a standard interstellar

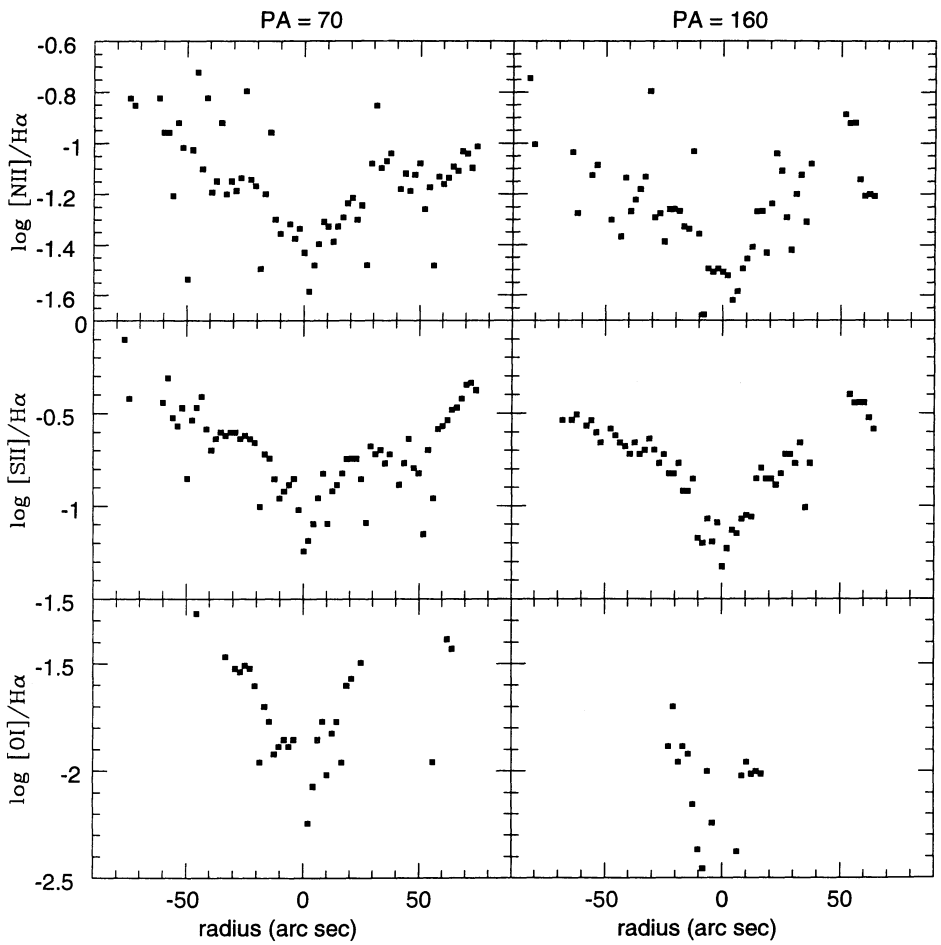

FIG. 7.—The log of the [N II] λ6584/Hα (*top boxes*), [S II] λλ6717 + 6731/Hα (*middle boxes*), and [O I] λ6300/Hα (*bottom boxes*) emission-line flux ratios plotted vs. location relative to super star cluster A. The data in P.A. = 70° (*left boxes*) have east-northeast to the left and west-southwest to the left. The data in P.A. = 160° (*right boxes*) have south-southeast to the left and north-northwest to the right. Note the systematic increase in all three ratios with increasing radius.

reddening curve, the corresponding intrinsic value is 0.04. Comparing this value to the photoionization models of Stasinska (1990) implies a mean temperature of $T_{\rm eff} \sim 35{,}000$ K for the ionizing radiation field. For individual main-sequence stars (Maeder 1990), this value of $T_{\rm eff}$ corresponds to stars with masses of only 20–25 $M_\odot$ (late O stars).

While it is possible that the initial mass function in NGC 1569 is peculiarly deficient in more massive stars, the more likely explanation for the relatively low $T_{\rm eff}$ is simply that the star-formation rate is declining steeply with time in NGC 1569 and that the hotter (i.e., more massive and hence shorter-lived) stars are no longer present in significant numbers. The main-sequence lifetime of a 20–25 $M_\odot$ star is about 7–9 Myr (Maeder 1990), so this interpretation would also be consistent with the paucity of Wolf-Rayet stars in this galaxy—which will disappear about 6–8 Myr after the cessation of star formation (Drissen et al. 1993). Israel (1988) has reached similar conclusions based on the far-UV colors of NGC 1569. A steep decline in the star-formation rate over the past 10 Myr is not inconsistent with the presence of numerous yellow and blue supergiants seen in the color-magnitude diagram published by Waller & Dracoby (1993). These have progenitor masses exceeding 20 $M_\odot$ and hence lifetimes of no more than 10 Myr.

This is not to say that stars more massive than 25 $M_\odot$ are entirely absent in NGC 1569, nor that star formation has completely ceased. Drissen & Roy (1994) have discovered a Wolf-Rayet star and its associated wind-blown nebula near the eastern end of the starburst. Waller (1991) inferred Hα emission-line equivalent widths of typically 10^3 Å for the brightest giant H II regions and their ionizing clusters. The models of Leitherer & Heckman (1995) for a starburst with quarter solar metallicity and a Salpeter IMF slope predict such equivalent widths for an upper mass cutoff of 30 $M_\odot$ and an age less than about 5 Myr. A higher upper mass cutoff is possible if dust is competing with gas for the ionizing photons in NGC 1569 (Waller 1990, p. 191).

4. DISCUSSION

4.1. *Starburst-driven Outflow in NGC 1569*

4.1.1. *Conceptual Overview*

As we emphasized in § 1, there is a broad theoretical consensus that starburst-driven outflows should occur in dwarf galaxies, and there is rather compelling optical evidence that such an outflow is indeed occurring in NGC 1569. This outflow is predicted to be a detectable source of thermal X-ray and optical line emission, and we believe that this is the most likely origin of the diffuse X-ray halo and Hα filaments in NGC 1569. We will therefore begin by briefly describing a simple model for a starburst-driven outflow in a dwarf galaxy, and by also summarizing the evidence that such an outflow is indeed occurring in NGC 1569. We will then consider the dynamics of the outflow in more detail in § 4.2, its application to the observed kinematics of the gas in § 4.3, and the origin of the X-ray and optical emission in § 4.4. Finally, we will consider the future development of the outflow and its possible influence on the evolution of NGC 1569 in § 4.5 (where we will also briefly discuss the implications for the evolution of dwarf galaxies in general).

We expect a galactic-scale outflow in the interstellar medium of a dwarf galaxy to occur when the kinetic energy supplied by supernovae and winds from massive stars in a starburst is efficiently thermalized (i.e., the collisions between stellar ejecta convert the kinetic energy of the ejecta into thermal energy via shocks, with little energy subsequently lost to radiation). As discussed by Vader (1987), Hensler, Theis, & Burkert (1993), and others, a quantitative assessment of the conditions under which such outflows can occur (and what their consequences will be) is a complex problem that depends on the multiphase nature of the ISM and the metallicity dependence of radiative cooling (among other factors).

The efficient thermalization of supernova energy is expected to occur when the (suitably normalized) kinetic energy input rate is so high that most of the *volume* (but not *mass*) of the starburst's ISM is filled by hot, tenuous supernova-heated gas (e.g., McKee & Ostriker 1977; Mac Low & McCray 1988; Norman & Ikeuchi 1989; Heiles 1990). These conditions are almost certainly met in dwarf starburst galaxies like NGC 1569—as has recently been discussed at length in MHWS. The collective action of an ensemble of supernovae and stellar winds would then create a "superbubble" of hot gas. Since its pressure is much larger than that of its surroundings, it will expand outward. As we will argue below (and see MHWS for details), the radiative cooling time in such an expanding bubble will likely be much longer than the bubble expansion time.

Such an expanding superbubble has an "onion-skin" structure of five concentric zones. From inide out these are: (1) an innermost region inside which the starburst injects mass and energy; (2) a region of supersonic outflow; (3) a region of hot gas. This is a combination of wind material from zone 2 that has passed through the internal shock that divides regions 2 and 3, mixed with material that has been evaporated by the hot gas off the inner edge of zone 4 and/or from interstellar clouds that have been overtaken and engulfed by the superbubble; (4) a thin, dense shell of ambient gas that has been swept-up, shocked, compressed, and then radiatively cooled as the "piston" of hot gas in zone 3 expands supersonically into the ambient medium; (5) the undisturbed ambient gas. In principle, much of the thermal X-ray emission could come from zone 3, while zone 4 should be a strong source of either optical and UV line emission or *soft* X-rays (depending on the speed at which the outer shock propagates into the undisturbed medium).

While the above spherically symmetric case may apply to some dwarf galaxies, the ISM in NGC 1569 (as mapped in H I) appears to have a more disklike structure. In this case, an expanding superbubble will expand most rapidly along the direction of the steepest pressure gradient (the disk's minor axis). During the early stages of its dynamical evolution the superbubble will have a structure similar to the above, but later it may "blow out" of the disk and assume a chimney-type topology (see Norman & Ikeuchi 1989; Mac Low & McCray 1988).

4.1.2. *Evidence for an Outflow in NGC 1569*

The presence in NGC 1569 of a diffuse X-ray halo which appears to be circumscribed by a system of expanding Hα filaments and immersed in an H I envelope is in good qualitative agreement with the above picture. Indeed, an ongoing kinematic survey of dwarf starburst galaxies with centrally concentrated starbursts (objects similar to NGC 1569) demonstrates that expanding superbubbles are common in this type of galaxy (see MHWS). In the case of NGC 1569, the most direct evidence that such an outflow is occurring is provided by data on the velocity field of the ionized gas. This has been traced by Faby-Perot data (de Vaucouleurs et al. 1974; de

Vaucouleurs 1981), by the long-slit spectra of TOS, and by our new long-slit spectra.

Both the Fabry-Perot data and our data (in P.A. 70) show a gradient in radial velocity along the minor axis (northeastern filaments redshifted and southwestern filaments blueshifted). In the biconic outflow model adopted by de Vaucouleurs, the deprojected outflow velocities would reach about 130 km s^{-1}. Our new data (which allow us to separate out the kinematics of the quiescent and high-velocity systems) reveal the presence of radial velocities of up to 200 km s^{-1} relative to v_{sys}. These velocities can be compared to the inferred rotation speed of the H I disk in NGC 1569 of only about 33 km s^{-1} at a radius of 1.3 kpc along the galaxy major axis (Reakes 1980). Thus, it is not possible for the much larger observed velocities in the Hα filaments to arise in gravitationally bound gas in polar orbits about the galaxy.

Our new spectroscopic data provide convincing additional evidence for an outflow of ionized gas in NGC 1569. The presence of the "Doppler ellipses" and their close correspondence with the large loops and filaments seen in the Hα image in Figure 1*c* implies that the extranuclear optical emission-line gas in NGC 1569 lies primarily along the surfaces of several large (kiloparsec-scale) bubble-like structures that are expanding at typical velocities of 100 ± 25 km s^{-1} (i.e., 150–250 km s^{-1} front-to-back velocity separation). We will henceforth refer to these expanding structures as "superbubbles." These superbubbles tend to lie primarily along the optical and H I minor axes of NGC 1569, as expected if they are expanding most rapidly along the direction of the steepest density gradient in the ISM.

Radio data provide additional indications of an outflow in this galaxy. The maps of the H I by Israel & van Driel (1990) show a 200 pc scale hole in neutral gas, centered on super star cluster A. This H I hole also encompasses (at least in projection) the compact X-ray sources 1 and 2 (which together comprise about 30% of the total X-ray emission from the galaxy), as well as a channel of depleted Hα emission (Waller 1991). Surrounding this channel are H II regions with streamlined morphologies, suggestive of a shearing interaction with the outflow (see Waller 1991). The kinematics of the H I are very disturbed just to the northwest of the H I hole, with a velocity range of about 100 km s^{-1} (compared to only 20–40 km s^{-1} elsewhere in the galaxy). Israel & Driel (1990) consider that the most likely explanation for the H I hole is that it has been evacuated by the kinetic energy supplied by multiple supernovae and stellar winds over the last 10 Myr or so. The hot gas venting out of this region may be responsible (at least in part) for producing the diffuse X-ray halo emission and for driving the expansion motions seen in the Hα filaments. There is also a prominent H I spur extending about 2.6 kpc to the south-southeast of the galaxy in the same region where a series of Hα arcs and a "blob" of X-ray emission are found (see Fig. 1*c*). It is possible that this H I spur has been transported out of the galaxy disk by the outflow, but better data on the H I kinematics are required to test this idea (Wilcots et al. 1995).

Radio continuum maps of NGC 1569 by Israel & de Bruyn (1988) reveal the presence of a nonthermal radio halo with a diameter of about 2 kpc. Such radio halos are relatively rare in star-forming galaxies and are believed to result when relativistic particles accelerated in the star-forming region are convected outward in a galactic wind or outflow (see Dahlem, Lisenfeld, & Golla 1995). Finally, as Waller (1991) has emphasized, indirect evidence that the starburst in NGC 1569 is driving an outflow is provided by the good agreement between the characteristic dynamical age of the Hα filament system and the various age estimates for the starburst based on UV, optical, and radio data. These ages (all of order 10^7 yr) are summarized in Table 5.

4.2. *The Dynamics of a Starburst-driven Superbubble*

4.2.1. *Energy Input from the Starburst*

In order to determine whether the expanding superbubbles in NGC 1569 can be plausibly driven by the observed population of massive stars, we need a good estimate of the rate at which such stars are supplying kinetic energy to the interstellar

TABLE 5

AGES AND TIMESCALES IN NGC 1569

$t_{I,H\alpha}$ (1)	$t_{I,UBV}$ (2)	$t_{C,H\alpha}$ (3)	$t_{C,UBV}$ (4)	t_{EF} (5)	t_{WR} (6)	t_{UV} (7)	t_{SSC} (8)	t_{dyn} (9)	t_{sync} (10)	t_{gas} (11)
6.8	6.7–6.8	7.2–8.5	7.1–7.5	7.3	>6.9	7.0	7.2	7.0	>6.7	8.7

NOTES.—Col. (1): Log of the age (in years) of a model of an instantaneous burst of star formation which matches the observed Hα equivalent width (see Table 1). The LF models of 25% solar metallicity were used, and all three IMFs they considered gave roughly the same age; col. (2): Same as col. (1), but the $(U-B)$ color was fit. The range shown corresponds to the three different IMFs considered by LH; col. (3): Same as col. (1), but the star formation in the model was assumed to be at a constant rate (the age is the time since the start of star formation). Different IMFs give different ages; col. (4): Same as col. (3), but the $(U-B)$ color was fitted; col. (5): Log of the age based on the UBV color vs. age relation measured by Elson & Fall 1988 for populous star clusters in the Large Magellanic Cloud; col. (6): A lower limit to log(age) for an instantaneous burst, based on the paucity of Wolf-Rayet stars (Drissen, Roy, & Moffat 1993; Drissen & Roy 1994). Note that the small value we measure for the flux ratio of the He I λ5876/Hα emission lines is consistent with this age as well (see text); col. (7): The log(age) based on the far-UV colors (Israel 1988); col. (8): The approximate log(age) derived for super star clusters A and B based on their spectroscopic properties (Prada, Greve, & McKeith 1994); col. (9): The log of the approximate dynamical timescale for the filament system (de Vaucouleurs, de Vaucouleurs, & Pence 1974), and see text; col. (10): The log of the time in the past at which the rate of injection of relativistic particles into the halo of NGC 1569 declined sharply (Israel & de Bruyn 1988). This is then a lower limit to the characteristic age of the starburst; col. (11): The log of the gas-depletion time (mass of neutral-plus-molecular gas divided by the star-formation rate implied by the "standard" LH model of constant star formation). The former is given in Table 1 and the latter is roughly 0.3 $M_\odot$ $year^{-1}$ for a Salpeter IMF extending from 0.1 to 100 $M_\odot$. See LH and text for details.

medium (hereafter L_{mech}) Either the Lyman continuum luminosity or bolometric luminosity of NGC 1569 can be used in principle to make this estimate (see Leitherer, Robert, & Drissen 1992 and Leitherer & Heckman 1995, hereafter LH). The Hα luminosity given in Table 1 implies a Lyman continuum luminosity of $Q = 3.5 \times 10^{52}$ s^{-1}, while Israel (1988) estimates the bolometric luminosity as $L_{bol} \sim 1.9 \times 10^9 L_\odot$.

The ratios between the rate of kinetic energy imput and either the bolometric or Lyman continuum luminosities will depend upon both the initial mass function (IMF) and the history of recent star formation in NGC 1569. We therefore considered three different initial mass functions modeled by LH and also considered two extreme models for the recent history of star formation in NGC 1569 (an instantaneous burst which occurred at some specified time in the past and a burst in which the star formation has occurred at constant rate from the start of the burst to the present time). We adopted the LH models for 25% solar metallicity, since this is a good match to the oxygen abundance in NGC 1569 (see Table 1).

Our specific procedure was then as follows. First we adopted either an instantaneous burst or a constant star-formation rate, and then selected one of three IMFs. These were: "normal" (Salpeter slope of -2.35 with an upper mass cutoff of 100 $M_\odot$), "truncated" (Salpeter slope with an upper mass cutoff of 30 $M_\odot$), and "steep" (slope $= -3.3$ and an upper mass cutoff 100 $M_\odot$). For each of these six possible combinations of star-formation history and IMF, we then estimated the ages at which the model best reproduced either the observed $(U-B)$ color or the global Hα emission-line equivalent width (see Table 1). While processes other than photoionization by hot stars can produce some of the observed Hα emission, we will show below that photoionization almost certainly dominates over mechanical heating in this regard. Thus using the Hα equivalent width as an age indicator should not be seriously affected by our neglect of these other processes.

The six models and two fitting parameters then provided 12 estimated ages. These were all ~ 6 Myr for the instantaneous-burst models and range from 13 to 31 Myr for the models of constant star formation. Such ages are plausible, as they correspond rather well to the various independent age estimates: (1) the expansion timescales for the Hα superbubble shells (see § 3.2.1 above), (2) the radiative loss time implied by the high-frequency steepening of the radio synchrotron spectrum (Israel & de Bruyn 1988), (3) the ages implied by the paucity of Wolf-Rayet stars and by the relatively cool effective temperature of the ionizing radiation (Drissen et al. 1993 and § 3.2.2 above), and (4) the estimated ages of super star clusters A and B (see Prada, Greve, & McKeith 1994).

For each of the 12 models, the prediction of the ratio of L_{mech}/L_{bol} for the appropriate starburst age was then multiplied by L_{bol} for NGC 1569 to provide one set of estimates of L_{mech}. We then repeated this procedure using the model ratio Q/L_{mech} and the measured value for Q for NGC 1569 to obtain another 12 estimates of L_{mech}. The set of 24 estimates of log L_{mech} range from 40.5 to 41.5 ergs s^{-1}, with a mean of 40.9 (8×10^{40} ergs s^{-1}).

Note that a population of massive stars will inject kinetic energy into the ISM at a roughly constant rate in two different circumstances (see Leitherer & Heckman 1995). First, following an instantaneous burst of star formation, L_{mech} will be roughly constant during the era from roughly 3–40 million yr (i.e., when Type II and Type Ib supernovae are occurring). This age range encompasses the age range we deduce on the basis of the instantaneous-burst model. Second, if the star formation occurs at a constant rate, L_{mech} will reach a roughly constant value after about 3×10^7 yr (again similar to age range we deduced based on the constant star-formation rate model). Thus, in our considerations of superbubble dynamics below we will assume—for simplicity—a constant rate of energy injection in NGC 1569. Of course, the future evolution of L_{mech} will differ in the case of an instantaneous burst compared to constant star formation. More detailed considerations of the consequences of the case in which the energy injection rate is not constant can be found in Koo & McKee (1992) and Shull & Saken (1995).

4.3. *Comparisons to a Simple Model*

The expansion of a superbubble may be driven by either the kinetic energy supplied by the starburst (in the event that radiative losses from the superbubble's interior are negligible) or by the momentum supplied by the starburst (if radiative losses are important). In the particular case of NGC 1569 we know that the observed X-ray luminosity of the halo of NGC 1569 is less than 1% of the rate at which the starburst injects kinetic energy. Moreover, the estimated radiative cooling time of the X-ray gas is considerably longer than the superbubbles' dynamical ages of $\sim 10^7$ yr, unless the volume filling factor of the X-ray gas is extremely small and its pressure is extremely high ($f < 10^{-3}$ and $P > 4 \times 10^{-10}$ dyn cm^{-2}, see Table 4). These comparisons suggest that radiative losses can be neglected in NGC 1569.

MHWS have recently considered the relative importance of radiative losses in a sample of superbubbles whose properties (and "host" galaxies) are very similar to NGC 1569. Their arguments are of a more theoretical nature than those above, and we briefly summarize them. First, they showed that the bulk of the volume of the ISM in the starburst is likely to be occupied by hot, tenuous gas (following the "porosity" formalism developed by McKee & Ostriker 1977). This means that most supernovae will detonate in low-density gas and will not suffer severe radiative losses. Second, they showed that the ratio of superbubble expansion time to radiative cooling time is probably very small, using the formalism of Mac Low & McCray (1988) for a superbubble expanding in a disk and that of Koo & McKee (1992) for a spherically symmetric situation. We refer the reader to MHWS for a more detailed discussion of the above considerations.

We therefore consider the dynamics of an adiabatic superbubble whose expansion is driven by the multiple supernovae and stellar winds occurring in its interior. For the range in L_{mech} deduced in § 4.2.1 above, the mean time between supernova explosions (100–1000 yr) is much less than the sound-crossing time inside a kiloparsec-scale hot superbubble (of order a million years). Thus we can treat the problem as one of steady injection of energy (i.e., as a wind-blown bubble) rather than as a series of impulsive events ("explosions"). This is of course only a rough approximation, rather than a fully realistic one. Furthermore, we will adopt a highly idealized model of a single superbubble that is being inflated into a spherically symmetric, single-phase medium of uniform density by energy that is being injected at a constant rate by an ensemble of massive stars distributed in a region whose size is much smaller than the current size of the superbubble. Since none of these specific assumptions are strictly true for NGC 1569, our aim here is not to develop a detailed model, but simply to show

that there is a rough consistency between the basic measured and predicted quantities.

For the simple case described above, the superbubble radius and velocity at a time t after the start of energy injection are given by (see Castor, McCray, & Weaver 1975):

$$r_{\rm Bubble} = 1.1 L_{\rm mech,41}^{1/5} n^{-1/5} t_7^{3/5} \ ({\rm kpc}) , \quad (1)$$

$$v_{\rm Bubble} = 65 L_{\rm mech,41}^{1/5} n^{-1/5} t_7^{-2/5} \ ({\rm km\ s^{-1}}) , \quad (2)$$

where $L_{\rm mech,41}$ is the kinetic energy injection rate in units of 10^{41} ergs s^{-1}, n is the number density (nucleons cm^{-3}) of the ambient gas, and t_7 is the time in units of 10^7 yr.

For NGC 1569, the models of either an instantaneous burst of star formation or a constant rate of star formation imply $L_{\rm mech,41} \sim$ unity (§ 4.2.1). The H I radio data imply $\langle n \rangle$ of order unity within a radius of 1.2 kpc (Israel & van Driel 1990). The overall size of the Hα filament system and X-ray halo (radius about 1.2 kpc) divided by the typical expansion speed of about 100 km s^{-1} implies a dynamical age of $t_7 \sim$ unity. This age is also consistent with various age estimates based on the optical and radio properties of NGC 1569 (see § 4.1.2 and Table 5).

Using these estimated parameters, our simple dynamical model predicts a spherical shell of gas with a radius of about 1 kpc expanding outward at about 60 km s^{-1}. In reality, NGC 1569 is considerably more complex (it is not a single spherically symmetric superbubble) and the observed expansion speeds are a bit larger than the above rough estimate ($\sim 100 \pm 25$ km s^{-1}). This latter disagreement could be remedied by adopting a model in which the ambient gas density $n(r)$ declined with radius and the superbubble accelerated as it expanded (see Koo & McKee 1992). This would be quite reasonable based on the H I map of NGC 1569 (Israel & van Driel 1990). Given the simplicity of the above model and the limited amount of available kinematic information, we regard the model and data to be in satisfactory agreement (see also Waller 1991).

As an additional comparison of this simple model to our data, we can compare the estimate of the thermal energy of the X-ray halo in Table 4 to the value predicted for an energy-conserving (adiabatic) superbubble. For $L_{\rm mech} \sim 10^{41}$ ergs s^{-1} integrated over a time of 10^7 yr (see above), the total energy injected by the starburst will be $\sim 3 \times 10^{55}$ ergs. Of this, about 1.4×10^{55} ergs will be in the form of thermal energy for an adiabatic bubble, which is consistent with the energy estimates in Table 4, provided the filling factor of the X-ray–emitting gas is near unity and the temperature is of order 10^7 K.

4.4. *Emission from the Superbubble*

4.4.1. *Thermal Models for the X-Ray Emission*

As described in § 4.1, X-rays from a wind-driven superbubble could in principle come from either the outer shell of shocked ambient gas (zone 4 in the notation of § 4.1) or from the bubble interior (zone 3)—see also Suchkov et al. (1994). The zone 4 material cannot contribute significantly in the particular case of NGC 1569 because the observed expansion speed of the superbubble system—$v_{\rm Bubble} \simeq 100$ km s^{-1}—corresponds in the adiabatic case to a postshock temperature in gas with a mean mass per particle μ of $kT = 3/16 \mu\ v_{\rm Bubble}^2 \sim 12$ eV ($T \sim 1.4 \times 10^5$ K). Such gas would be much too cool to emit significantly in the *ROSAT* HRI bandpass. Moreover, the morphology of the X-ray halo is not limb-brightened, as would be expected in such a picture.

Thus in NGC 1569 most of the thermal X-ray emission from the outflow presumably arises from material in zone 3. As noted in § 4.1, this material is a combination of wind fluid from zone 2 that has passed through the internal shock that divides regions 2 and 3, mixed with material that has been evaporated by the hot gas off the inner edge of zone 4 and/or from interstellar clouds that have been overtaken and engulfed by the superbubble. Let us first briefly consider the simplest possible case in which we neglect evaporation. As we will argue below, this situation corresponds to the minimum X-ray luminosity expected for zone 3 (and the maximum temperature).

For an adiabatic bubble blown by a wind with a mechanical luminosity $L_{\rm mech}$ and a mass outflow rate $\dot{M}$, the approximate X-ray temperature will be $T_x = (5/11) T_0$, where $T_0 = 2/3 (L_{\rm mech}/\dot{M})\ \mu/k$ (see Koo & McKee 1992). For a starburst-driven superbubble, we estimate that $T_x \sim 8.5 \times 10^7$ K (7.3 keV)—see LH. To estimate the characteristic X-ray luminosity of the bubble, we will assume that the shocked wind fluid uniformly fills the entire interior volume of the bubble (i.e., we assume that the relative volumes occupied by zones 1 and 2 are negligible). As discussed by Koo & McKee (1992), this assumption will be valid for the case we are considering in which the velocity of the wind fluid in zone 2 (~ 2800 km s^{-1}—see LH and Chevalier & Clegg 1985) is much greater than the expansion speed of the outer bubble shell (~ 100 km s^{-1}). The approximate X-ray luminosity in the *ROSAT* 0.1–2.4 keV energy band will then be

$$L_x \sim 1.7 \times 10^{37} L_{\rm mech,41}^{7/5} t_7^{1/5} n^{3/5} \ ({\rm ergs\ s^{-1}}) , \quad (3)$$

while the gas pressure inside the superbubble will be

$$P_{\rm Bubble} \sim 7 \times 10^{-11} L_{\rm mech,41}^{2/5} t_7^{-4/5} n^{3/5} \ ({\rm dyn\ cm^{-2}}) . \quad (4)$$

Taking the values we have estimated above as appropriate to NGC 1569 ($L_{\rm mech,41} \sim t_7 \sim n \sim$ unity), we find that the predicted X-ray luminosity of the no-evaporation model is roughly an order of magnitude lower than the acutal value for the diffuse halo ($\sim 4 \times 10^{38}$ ergs s^{-1}, using the ECF appropriate to gas with $kT \sim 5$ keV—see § 2.1.2). The predicted pressure is consistent with the upper limit on the pressure measured in the optical emission-line filaments ($< 3 \times 10^{-10}$ dyn cm^{-2}) but is inconsistent with the lower limits for the pressure in the X-ray halo unless the temperature is less than a few keV. Such a low temperature is in turn inconsistent with the predicted temperature of ~ 7 keV for the no-evaporation model (see above and Table 4).

The above discrepancies are most likely due to our neglect of evaporation. The effect of evaporation will be to increase the mass of hot gas while decreasing its mean temperature. Since the emissivity per gram of hot gas in the *ROSAT* energy band is insensitive to temperature in the range $\log T = 6$–7 and actually falls with increasing temperature for $\log T = 7$–8 (see Suchkov et al. 1994), evaporation—which will increase the mass and density of the X-ray–emitting material—will result in an increase in the *ROSAT*-band X-ray luminosity. A detailed quantitative treatment of the effect of evaporation on L_x is not straightforward, since the theory of mass exchange between different phases in the ISM is not well developed and depends on a host of poorly constrained parameters (see Hartquist & Dyson 1993).

Mac Low & McCray (1988) have considered the particular case in which classical conductive heating results in the evaporation of zone 4 material and its subsequent mixing with the hot material in zone 3. Their similarity solution for the radial

variation in the temperature and density inside the superbubble is

$$T(R) = 1.7 \times 10^7 L_{\rm mech,41}^{8/35} n^{2/35} t_7^{-6/35} (1 - R)^{2/5} \text{ K}, \quad (5)$$

$$N(R) = 0.012 L_{\rm mech,41}^{6/35} n^{19/35} t_7^{-22/35} (1 - R)^{-2/5} \text{ (cm}^{-3}), \quad (6)$$

where R is the radial coordinate in units of the radius of the superbubble's outer shell. The total gas mass inside the shell is given by

$$M(R) = 4.9 \times 10^6 L_{\rm mech,41}^{27/35} n^{-2/35} t_7^{41/35} \ (M_\odot). \quad (7)$$

Integrating over the bubble volume using the 0.1–2.4 keV emissivity in Suchkov et al. (1994), we obtain

$$L_x \sim 5 \times 10^{39} L_{\rm mech,41}^{33/35} n^{17/35} t_7^{19/35} \text{ (ergs s}^{-1}), \quad (8)$$

where we have taken a constant emissivity for $T_0 > T > 10^6$ K and an emissivity of 0 for $T < 10^6$ K (see Suchkov et al. 1994). This value is about an order of magnitude *greater* than we measure for the halo, but the estimate is rather sensitive to the low-temperature cutoff in the above integration. For example, ignoring the emission from gas cooler than $T = 6 \times 10^6$ K (in view of the large foreground Galactic column density and the small effective area of the HRI at low energies—see § 2.1) drops the predicted luminosity by a factor of ~ 3.

Thus we see that the inclusion of evaporation can potentially increase the predicted X-ray luminosity by a significant factor. Evaporation could also allow us to reconcile the observed and predicted pressures inside the superbubbles. Since evaporation will lower the temperature of the gas, the estimate of the pressure based on the *ROSAT* data will also drop. As can be seen in Table 4, the lower limits to the pressure in the X-ray halo are consistent with the predictions of equation (4) above as long as $kT <$ few keV. Note also that while equation (4) was derived ignoring evaporation, inclusion of this process will not significantly change the predicted pressure (since, by energy-conservation arguments, the volume integral of pressure will be conserved).

4.4.2. *Inverse Compton X-Ray Emission*

NGC 1569 possesses a bright radio halo (Israel & de Bruyn 1988), produced by synchrotron emission from a population of relativistic electrons that have probably flowed out of the starburst. Since there is also a copious supply of "soft" (ultraviolet, optical, and infrared) photons produced by the starburst, we expect that inverse Compton scattering of these soft photons by the relativistic electrons will lead to nonthermal X-ray emission from the halo (see Schaaf et al. 1989). It is therefore important to make a rough estimate of the expected inverse Compton X-ray luminosity.

An estimate of this luminosity follows from elementary considerations. The ratio of the inverse Compton and synchrotron luminosity of a plasma with a magnetic field energy density $U_{\rm mag}$ ($= B^2/8\pi$) bathed in a radiation field with energy density $U_{\rm rad}$ is just the ratio of $U_{\rm rad}$ to $U_{\rm mag}$ (see Shu 1991). Israel & de Bruyn (1988) derive a value of $U_{\rm mag} = 5.7 \times 10^{-12}$ ergs cm^{-3} for standard "minimum energy" conditions in the halo synchrotron source (see Miley 1980). We approximate $U_{\rm rad}$ in the halo as that given by the galaxy bolometric (UV + optical + infrared) luminosity, assuming this arises in a point source at the center of the halo. Adopting a more realistic model of a spatially extended source of this radiation does not significantly affect our calculation, since the radio halo is significantly larger than the galaxy half-light radius—see Table 3. Thus, using $L_{\rm bol}$ from Table 1, we obtain

$$U_{\rm rad} \sim L_{\rm bol}/(4\pi c r^2) = 2.2 \times 10^{-12} r_{\rm kpc}^{-2} \text{ (ergs cm}^{-3}), \quad (9)$$

where $r_{\rm kpc}$ is the radial distance into the halo in kpc. Taking this law for the radial dependence of $U_{\rm rad}$ and the above value for $U_{\rm mag}$, we can integrate over radius to obtain a predicted inverse Compton luminosity:

$$L_{\rm IC} = 0.86 L_{\rm syn} \left(\frac{r_{\rm rad}}{1 \text{ kpc}} \right) = 1.2 \times 10^{37} \text{ (ergs s}^{-1}), \quad (10)$$

where $r_{\rm rad}$ is the radius of the radio halo (1.1 kpc—see Table 3). We have used $L_{\rm syn} = 1.3 \times 10^{37}$ ergs s^{-1}, which is the total radio luminosity integrated over the frequency range from 10 MHz to 8 GHz (Israel & de Bruyn 1988).

Note that this estimate refers to the total inverse Compton luminosity, only a fraction of which will be emitted in the *ROSAT* bandpass. If one uses the ECF appropriate to the inverse Compton model (a power law with $\Gamma = 1.7$—see § 2.1.2), the total X-ray luminosity of the halo + "southern blob" is 5.6×10^{38} ergs s^{-1}. We thus conclude that inverse Compton emission will make only a minor contribution to the observed X-ray emission. There is, however, one caveat: the estimate of $U_{\rm mag}$ (and hence of $L_{\rm IC}$, which is inversely proportional to $U_{\rm mag}$) assumes "minimum energy" conditions in the radio halo. It is possible that the radio halo is far from these conditions and that the energy density in the magnetic field is significantly smaller than the value we adopted above. The observed radio emission would then require a much larger total energy in the form of relativistic particles in the halo. In this case, the inverse Compton luminosity would be proportionately larger than our above estimate. Such a situation seems unlikely, however, since even the "minimum energy" assumption implies a total energy in the radio plasma of 4.4×10^{54} ergs (Israel & de Bruyn 1988). This is already of order 10% of the total kinetic energy output of the supernovae in the starburst over the last 10^7 yr (see § 4.2.1), so a halo with much larger total energy and inverse Compton luminosity is implausible.

4.4.3. *Powering the Optical Line Emission*

Having discussed the origin of the X-ray halo emission, we now briefly consider the heating source for the optical emission-line nebula. As noted in § 4.1, the shocked ambient gas encountered by the expanding bubble (i.e., gas in zone 4) should cool radiatively, and this shocked gas may contribute significantly to the Hα emission from the filaments. The typical expansion velocities of the superbubbles in NGC 1569 are about 100 km s^{-1}. The shock models of Shull & McKee (1979) predict that shocks with this velocity will produce roughly 0.5 Hα photons per shocked proton. Thus, we estimate that the Hα luminosity due to shocks alone of a superbubble with radius r expanding into an ambient medium with density n at a velocity v will be $L(\text{H}\alpha) \sim 4\pi(r^2 nv) 0.5 h\nu_{\text{H}\alpha} \sim 2 \times 10^{39}$ ergs s^{-1} for $r = 1$ kpc and $n =$ unity. This is only 5% of the total observed Hα luminosity of NGC 1569, but about 20% of the luminosity of the high-velocity system. This suggests that photoionization is the predominant heating source for the emission-line gas as a whole, but that shocks are likely to make a nonnegligible contribution to the optical emission in the low surface brightness outer filaments, where high gas velocities and relatively large ratios of [O I]/Hα, [N II]/Hα, [S II]/Hα are observed. We emphasize, however, that the observed line ratios are too low in the filaments to be consistent with *pure* shock-heating (see Shull & McKee 1979).

The predominance of photoionization is not at all surprising, since the ratio of the kinetic energy injection rate to the luminosity of the ionizing radiation in starbursts is predicted to be only 5%–10% for the range in IMFs and starburst ages we have considered for NGC 1569 (see § 4.2.1 above and LH). If the gas is predominantly photoionized, then the relatively strong [O I], [N II], and [S II] lines in the halo filaments could be attributed to either the additional heating provided by shocks, or to the very dilute radiation field provided by the starburst. Waller (1991) has also suggested that both shocks and photoionization by dilute starlight may play an important role in exciting the filaments in NGC 1569.

In photoionized gas, as the local ratio of ionizing photons to electrons (the so-called ionization parameter U) decreases, the relative strengths of lines produced by low-ionization species like O I, N II, and S II increase (see Sokolowski 1995). Since the size of the starburst is much smaller than that of the filament system, the number density of ionizing photons will drop with radius as r^{-2} at large radii (and even more steeply if the effects upon the Lyman continuum of radiative transfer are included). Thus, we would expect the relative strengths of emission lines from low-ionization species to increase with increasing radius.

Models for superbubbles (see above) imply that the gas pressure in zones 3 and 4 should be roughly constant. Since photoionized gas has a fairly narrow range of equilibrium temperature ($\sim$5000–20,000 K—see Osterbrock 1989), we would therefore expect that the density in the filaments would also be roughly constant. Thus, the ionization parameter U should drop steeply with distance from the starburst. If we use the predicted pressure inside the superbubble from equation (4) above and assume that the filament gas is fully ionized with $T \sim 10^4$ K, then the estimated Lyman luminosity of $Q = 3.5 \times 10^{52}$ s^{-1} in NGC 1569 implies a predicted ionization parameter in the filaments of

$$U(r) = 3.3 \times 10^{-4} r_{\rm kpc}^{-2} L_{\rm mech,41}^{-2/5} t_7^{4/5} n^{-3/5} . \quad (11)$$

This estimate is valid as long as r is much larger than the size of the starburst and the effects of radiative transfer are small (the latter assumption makes it an upper limit on U).

Sokolowski (1995) has constructed a grid of models for gas photoionized by the diffuse radiation field of an ensemble of massive stars having either a Salpeter or Miller-Scalo IMF. These models predict that [S II] $\lambda\lambda$6717+6731/Hα rises from 7% for log $U = -2$ to about 80% for log $U = -4$, while [N II] λ6584/Hα rises from 7% to 65%, and [O I] λ6300/Hα rises from 1% to 12%. Taking log $U = -3$ as the typical value expected for the filaments, the model predicts [S II]/H$\alpha \sim$ 30%, [N II]/H$\alpha \sim$ 40%, and [O I]/H$\alpha \sim$ 4%. The predicted values for the [S II]/Hα and [O I]/Hα ratios agree roughly with the typical observed values in the filaments, but the observed [N II]/Hα ratio is typically a factor of about 5 smaller than predicted by the model. Since these models were for gas with solar metallicity (vs. an oxygen abundance of $\sim\frac{1}{4}$ solar in NGC 1569), and since there may be a trend for the abundance ratio of N/O to decline with declining metallicity in galaxies (see Pagel & Edmunds 1981), a more detailed quantitative comparison to the data is probably not warranted.

4.5. *The Future Evolution of NGC 1569: Implications for Dwarf Galaxies*

4.5.1. *The Role of Mass Loss in Evolutionary Models*

The most interesting issue raised by our data concerns the ultimate effect that the observed outflow will have on the subsequent evolution of NGC 1569. This is particularly important in view of the widespread invocation of the process of starburst-driven mass loss as a crucial mechanism in theories of the evolution of dwarf galaxies.

In some such theories, the wholesale ejection of the ISM and a long-term change in the galaxy's structure and/or Hubble type is involved (see Saito 1979; Babul & Rees 1992). That is, the loss of a significant fraction of the galaxy mass causes the galaxy to expand (and its surface brightness to drop), while the loss of the interstellar medium shuts off future star formation, thereby allowing the galaxy to rapidly fade and redden (see Arimoto & Yoshii 1986). Thus, the operation of a starburst-driven galactic outflow may result in the transmutation of one type of dwarf galaxy into another (e.g., NGC 1569 could be transmuted into a dwarf elliptical galaxy). In other evolutionary theories (see De Young & Gallagher 1990; Lynden-Bell 1992), the bulk of the cold ISM in the galaxy may be retained following the starburst, but the hot highly metal-enriched gas injected by the starburst vents out of the ISM and is lost from the system (thus changing the galaxy's chemical evolution). More complex scenarios which consider a two-phase ISM (Hensler et al. 1993) allow continuing star formation and a consequent long-lived outflow of gas and metals.

To better understand the distinction between these classes of theories, it is important to distinguish between the fate of the hot gas in the interior of the superbubble (zones 1 through 3 in the notation of § 4.1) that is directly supplied by the supernovae and stellar winds in the starburst, and the relatively cool and dense shock-heated and accelerated ambient gas in the superbubble shell (zone 4). In theories in which the starburst blows away the preexisting ISM, the cool gas in zone 4 must ultimately encompass the bulk of the ISM and must be accelerated to beyond the escape velocity. In theories in which only the metals created by the starburst are ejected, only the hot gas in zones 1 through 3 needs to escape. This can occur if the shell of gas in zone 4 ruptures before this shell has been accelerated to beyond the escape velocity.

It is also important to remember that the simple expanding-bubble model described above ignores the two-phase nature of the ISM. In the (not unlikely) event that most of the ISM mass is in the form of clouds that occupy a relatively small fraction of the volume, the expanding superbubble will propagate through the tenuous intercloud medium. This will overtake, compress, crush, and ultimately destroy the clouds. As noted above, such material may make a dominant contribution to the observed X-ray emission. The inclusion of a two-phase ISM allows a richer and more complex suite of possible evolutionary paths. For example, the tenuous intercloud gas might be ejected, but the most massive and dense clouds could be retained. This might allow star formation to continue even in the aftermath of a powerful starburst. Given that there is a no detailed physical understanding of how mass exchange between the different phases of the ISM occurs (see Hartquist & Dyson 1993), it is difficult to draw firm quantitative conclusions about the outcome of such a process. Some important steps in this direction are now in progress (Hensler et al. 1993; Berman & Suchkov 1991).

4.5.2. *Blowout and the Chemical Evolution of NGC 1569*

As noted above, supernova-driven outflow models have been used to explain the low metal abundances in dwarfs. Here the most important requirement is that the outflow suceeds in ejecting the newly formed metals, and it is less important that

the general interstellar medium of the dwarf be ejected. To see one way in which this process may occur, we can consider how the superbubbles in NGC 1569 are likely to evolve dynamically in the simple picture of a single-phase ISM. As we have emphasized above, the process by which metals are ejected could be quite different for a two-phase ISM in which most of the mass is in the form of dense, massive clouds (see Hensler et al. 1993).

Equation (2) above implies that the superbubble's outer shell (zone 4) will decelerate with time, even if energy continues to be injected at a constant rate. This is an artifact of adopting a constant density for the ambient medium. As a more realistic model, we can consider a superbubble being inflated by a starburst located at the midplane of a plane-parallel stratified atmosphere (e.g., the gaseous disk of NGC 1569). The superbubble will then expand most rapidly along the direction normal to the plane of the disk. For an exponential density law in the vertical direction, the expanding superbubble's shell will accelerate with time once its radius is several disk scale heights (see Mac Low & McCray 1988). In this case, since the effective gravity in the shell is directed inward, and since the dense shell overlies a more tenuous interior, it is expected that Rayleigh-Taylor instabilities will cause the shell to fragment, allowing the hot tenuous fluid inside the superbubble to then escape from the ruptured superbubble. This process is referred to as "blowout." Following blowout, the hot gas injected inside the starburst could vent directly out of the galaxy and be lost. In order for blowout to occur, the superbubble must therefore be able to accelerate outward rather than stalling, and there must be enough time for Rayleigh-Taylor instabilities with sizes as large as the thickness of the superbubble wall to grow. We can briefly consider these two requirements in turn.

Mac Low & McCray (1988) have shown that a superbubble will blow out of a disklike ISM having a scale height of H (in kpc) and a pressure P/k (in units of 10^4 K cm^{-3}) if the dimensionless rate of kinetic energy injection $L > 100$, where

$$L = 10^4 L_{\rm mech,41} H_{\rm kpc}^{-2} P_4^{-3/2} n^{1/2} . \quad (12)$$

Our estimated values for these parameters are $L_{\rm mech,41} \sim$ unity, $H_{\rm kpc} \sim 0.5$ (based on the H I maps in Israel & van Driel 1990), $P_4 \sim 0.03$ (assuming the pressure scales with the specific binding energy of the ISM and that $P_4 \sim$ unity in the Galactic ISM), $n \sim$ unity. Thus, we find that $L \sim$ several $\times 10^6$. It therefore appears very likely that the observed superbubbles will ultimately blow out of this galaxy.

For the superbubble shell to fragment via Rayleigh-Taylor instabilities, density perturbations with sizes at least comparable to the thickness of the superbubble shell ($\Delta r_{\rm Bubble}$) must have had time to grow. We therefore take the relevant Rayleigh-Taylor timescale to be $t_{\rm RT} \sim (\Delta r_{\rm Bubble}/2\pi g)^{1/2} \sim (\Delta r_{\rm Bubble} t_{\rm exp}/2\pi v_{\rm Bubble})^{1/2}$, where g is the net acceleration of the bubble wall (which we approximate by the current bubble expansion speed $v_{\rm Bubble}$ divided by the expansion timescale for the bubble $t_{\rm exp}$). We have simplified this expression by assuming that the ratio of the densities in the bubble wall and interior is much larger than unity. Taking typical parameters to be $\Delta r_{\rm Bubble} = 0.1$ kpc, $v_{\rm Bubble} = 100$ km s^{-1}, and $t_{\rm exp} \sim 10^7$ yr, we estimate that $t_{\rm RT} \sim 10^6$ yr, which is about an order of magnitude shorter than the superbubble expansion timescale.

The morphology of the X-ray and Hα image and optical spectra can provide clues as to whether blowout has already occurred in NGC 1569. We would then expect to see open-ended radially oriented filaments rather than closed loops in the Hα image, and likewise the long-slit spectra would show double-peaked or multicomponent emission-line profiles off the galaxy center, but no closed Doppler ellipses. While no firm conclusions can be drawn from the images and spectra shown in Figures 1 through 3, the morphology and kinematics of the ionized gas suggest that blowout has not occurred yet. The X-ray image is consistent with this inference, since the hot gas is neatly circumscribed by the system of expanding Hα filaments rather than protruding well beyond the Hα filaments (as in the case of M82—see Fabbiano 1988).

4.5.3. *Will the ISM Be Ejected in NGC 1569?*

A more dramatic possibility than blowout is that the starburst in NGC 1569 will succeed in blowing away the bulk of the ISM, thereby radically changing the future evolution of the galaxy. For this to be possible, the energy supplied by the starburst must be adequate to accelerate the ISM to a velocity greater than the escape velocity.

The escape velocity can only be roughly constrained, since we do not have measurements of the extent of the galactic potential. Taking a spherically symmetric isothermal potential with an outer cutoff at $r_{\rm max}$ and a depth corresponding to the square of the circular orbital velocity ($v_{\rm circ}^2$), then the escape velocity for material at a radius r is just (see Binney & Tremaine 1987)

$$v_{\rm esc}(r) = \sqrt{2}\, v_{\rm circ}[1 + \ln(r_{\rm max}/r)]^{1/2} . \quad (13)$$

The rotation curve for H I in NGC 1569 (Reakes 1980) implies that the rotation speed is about 33 km s^{-1}. Taking this value as characterizing the isothermal halo then implies that the escape velocity at the location of the outer edge of the Hα filament system (a radius of about 1.7 kpc) would be $\sim$47 km s^{-1} and $\sim$85 km s^{-1} for $r_{\rm max} = 1.7$ kpc and 17 kpc, respectively (where the latter might be appropriate if NGC 1569 had an extensive dark matter halo—see Meurer 1994).

Comparing the estimated escape velocity to the typical superbubble expansion velocities of about 100 km s^{-1} and to the extreme observed velocities of over 200 km s^{-1}, it appears likely that gas will be ejected from NGC 1569. How much gas can the starburst ultimately eject? The total mass of atomic and molecular gas in NGC 1569 is roughly $1.7 \times 10^8\ M_\odot$ (Israel 1988). The starburst models of LH that provide acceptable fits to NGC 1569 (see § 4.2.1) imply that the total kinetic energy that will ultimately be injected by the starburst is roughly $\log E = 55.7$ for the instantaneous-burst model and $\log E \gtrsim 56.2$ for the constant star-formation rate model (where the lower limit assumes that no further star formation occurs). Mac Low & McCray (1988) and Koo & McKee (1992) show that for an adiabatic bubble inflated by a constant rate of energy injection and expanding into a medium of constant density, roughly 20% of the injected energy resides in the kinetic energy of the swept-up shell (zone 4). Thus, the starburst could accelerate the ISM in NGC 1569 to a velocity of roughly 80 km s^{-1} for the instantaneous-burst model and $\gtrsim$140 km s^{-1} for the constant star-formation rate model. We therefore conclude that the starburst in NGC 1569 is energetically capable—at least in principle—of ejecting the galaxy's entire ISM.

Whether this will actually occur is far more problematic and will depend strongly on the geometry and multiphase nature of the ISM in NGC 1569. We have briefly discussed the latter above. De Young & Heckman (1994) have considered the spe-

cific problem of the role of geometry in determining whether centrally concentrated starbursts can eject the ISM of a low-mass galaxy like NGC 1569. The parameters they consider are: (1) a specified galaxy mass and radius (an implicit escape velocity), (2) the ellipticity of the ISM (with a sphere and a flat disk being the limiting cases), (3) the mean density of the ISM (an implicit ISM mass, given an assumed galaxy size and ellipticity), and (4) the total kinetic energy injected by the starburst.

Provided that the amount of kinetic energy provided by the starburst per unit mass of ISM is sufficient in principle to unbind the gas—as appears to be the case in NGC 1569—they find that the next most important parameter is the ellipticity of the ISM. That is, for the same ISM mass and amount of injected energy, flattened ISMs are more difficult to blow away. This is because the superbubble inflated by the starburst tends to quickly blow out along the minor axis. If blowout occurs rapidly ($\ll 50$ Myr), then the starburst imparts relatively little acceleration to the gas in the outer portions of the gas disk's equatorial plane (the energy and momentum instead flows out along the minor axis). In this case, the outer disk of the ISM can be retained by the galaxy even though the starburst provides enough kinetic energy to unbind it in principle.

Thus a starbursting dwarf galaxy may be better able to retain much of its ISM than simple energetic arguments suggest (either through geometrical effects or by virtue of a multiphase ISM which contains sufficiently robust clouds). This would be consistent with the fact that some of the dwarf and low-mass galaxies in the Local Group have apparently experienced two or more major episodes of star formation (e.g., Mateo 1992; DaCosta 1992; Lehnert et al. 1992; Smecker-Hane et al. 1994). This also leads to the possibility of cyclic starburst episodes in NGC 1569 (Waller 1991) and other similar systems.

We can summarize our inferences in § 4.5 as follows. The observed expansion velocities of the superbubbles exceed the likely escape velocity in NGC 1569. Moreover, the total amount of kinetic energy that the starburst will inject appears adequate to accelerate the entire ISM of NGC 1569 to near or beyond escape velocity. Thus it is possible that these superbubbles will ultimately eject this galaxy's ISM. Alternatively, the superbubbles may blow out along the minor axis of the ISM before the bulk of the gas in the outer galaxy disk has been significantly accelerated (see De Young & Heckman 1994). It is also possible that NGC 1569 can retain sufficiently robust interstellar clouds while losing its tenuous intercloud medium. However, even if NGC 1569 is able to retain the bulk of its ISM, most of the hot material from the superbubble interior will probably escape. In this case, the newly synthesized metals formed by the massive stars in the starburst would be lost from the galaxy.

5. SUMMARY AND IMPLICATIONS

In the present paper, we have presented and discussed both new *ROSAT* observations of the hot X-ray–emitting gas in NGC 1569 and new long-slit optical spectra that probe the kinematics and physical state of the famous emission-line filament system. We find that over half the X-ray emission detected in our *ROSAT* HRI image of NGC 1569 originates in a diffuse, nonspherical halo that can be detected out to a maximum radius of about 1.9 $\sim$1.2 kpc and has a luminosity of $\sim 3 \times 10^{38}$ ergs s^{-1} in the *ROSAT* 0.1–2.4 keV band. This diffuse X-ray emission is preferentially elongated along or near the minor axis of the flattened distribution of the stars and H I in the galaxy.

The diffuse X-ray emission bears a close morphological relationship to the Hα filament system. The filaments seem to define the surfaces of several large (kiloparsec-scale) structures (superbubbles) with the diffuse X-ray emission arising from the interiors of the cavities. Our long-slit optical spectra taken through the Hα filaments show that the emission-line profiles within these structures are double or multiply peaked, and the kinematics are consistent with them being cavities expanding at typical velocities of ± 100 km s^{-1} (i.e., a velocity splitting of 200 km s^{-1} in the emission-line profiles). Apparent outflow speeds of up to 200 km s^{-1} are present at some locations. The dynamical ages of these structures (roughly 10^7 yr) are quite similar to several independent estimates of the age of the starburst in NGC 1569. We also see a much more quiescent kinematic component in NGC 1569 in which velocities are everywhere within about 30 km s^{-1} of $v_{\rm sys}$. This component is located within the centralmost kpc of the galaxy and presumably corresponds to gas in the starbursting disk. We estimate that this quiescent material produces about 74% of the total Hα emission from NGC 1569, while the high-velocity gas associated with the expanding superbubbles comprises the remainder. We also found very broad wings (full width at zero intensity of 1400–2300 km s^{-1}) on the Hα emission-line profile centered on super star cluster A, suggestive of recent supernova activity there.

We have shown that the morphology, luminosity, and physical characteristics of the diffuse X-ray halo and the morphology, luminosity, kinematics, and age of the Hα filament system are all consistent with the expectations of an outflow driven by the starburst in NGC 1569. In such a model, the kinetic energy supplied by supernovae and stellar winds creates a region of hot gas whose pressure is very much greater than that of its surroundings. This hot gas will therefore expand most rapidly along the direction of the steepest pressure gradient in the ISM (along the minor axis of the galaxy disk) inflating a pair of "superbubbles" that extend out along the galaxy minor axis. The dense gas in the expanding outer walls of the superbubbles will be photoionized by the starburst and will also be shock-heated, making it emit copiously in Hα. Moreover, as gas newly heated in the starburst flows out into the expanding superbubbles, it will be shock-heated to temperatures in excess of 10^7 K. Thus the interior of a superbubble is expected to be a detectable source of keV X-rays circumscribed by an outer shell of Hα-emitting material.

To evaluate this picture more quantitatively, we have considered an idealized "toy" model of a single spherically symmetric superbubble being inflated into a medium of constant density by the kinetic energy supplied by a centrally concentrated starburst. We have considered an "energy-driven" rather than a "momentum-driven" superbubble, since several independent arguments imply that radiative losses can probably be neglected in NGC 1569. We have estimated the kinetic energy injection rate provided by the starburst in NGC 1569 by using state-of-the-art starburst models combined with observational estimates of the Lyman and bolometric luminosities of its massive stellar population.

Our toy model predicts a size and an expansion speed for the superbubble that agree reasonably well with the observed properties of the Hα filaments. The predicted pressure inside the superbubble is consistent with the observational constraints on the pressure in the emission-line filaments and

diffuse X-ray halo. The minimum predicted X-ray luminosity of the superbubble (by a "no evaporation" model) is about an order of magnitude smaller than is observed. The inclusion of X-ray emission from gas that has been evaporated off dense ambient material by the hot gas inside the superbubble can dramatically boost the predicted X-ray luminosity. We have considered the possibility of inverse Compton X-ray emission from the relativistic particles in the radio-synchrotron halo. We found that this process will make only a minor contribution to the X-ray emission, unless the radio halo is far from "minimum energy" conditions. This seems implausible, since the minimum energy of this radio plasma is already about 10% of the total energy injected by supernovae over the last 10^7 yr.

The luminosity of the Hα filament system implies that it is primarily excited by the radiation from the starburst. Shock heating associated with the outflow may also contribute and could be responsible in part for the relatively large ratios of [O I] λ6300/Hα and [S II] $\lambda\lambda$6717, 6731/Hα observed in the filaments. Such ratios can also be produced by photoionization by the very dilute radiation field produced by the starburst.

We have considered the relevance of the outflow observed in NGC 1569 to theories for the evolution of dwarf galaxies. Some theories contend that a powerful starburst will actually eject most or all of the interstellar medium of a dwarf galaxy, with devastating consequences for the future evolution of the galaxy. In this vein, we have emphasized that the filament system and X-ray halo have sizes comparable to the overall optical and H I dimensions of NGC 1569, and so are of global proportions in this small galaxy. The expansion velocities seen in the Hα filament system probably exceed the (rather uncertain) escape velocity in NGC 1569. Moreover, the total amount of kinetic energy that will ultimately be injected by the starburst ($\sim 10^{56}$ ergs) is sufficient in principle to accelerate the entire observed ISM to near or beyond the escape velocity. However, we have also stressed that the amount of mass that will ultimately be ejected from NGC 1569 is a sensitive function of the geometry and multiphase nature of the ISM (see below) and of the extent of any dark matter halo that may be present.

We have also discussed theories in which starburst-driven outflows strongly influence the chemical evolution of dwarf galaxies but do not eject the bulk of the galaxy's interstellar medium. In such theories, only the very hot X-ray–emitting fluid inside the superbubble (which contains the metals that have been newly synthesized by the starburst) escapes from the galaxy. Various hydrodynamical models have suggested that this can occur if a superbubble shell accelerates outward and fragments, allowing the hot gas inside to "blow out" of the galaxy (see Mac Low & McCray 1988). As discussed by De Young & Heckman (1994), if a centrally concentrated starburst occurs in a suitably flattened (disklike or oblate) ISM, blowout along the minor axis can allow the bulk of the ambient gas far out in the equatorial plane of the disk to be retained by the galaxy. For a multiphase ISM, it is also possible to eject the tenuous intercloud medium while retaining suitably massive and robust gas clouds. The ability of the galaxy to retain a significant fraction of its ISM would be consistent with the fact that some of the dwarf and low-mass galaxies in the Local Group have apparently experienced two or more major episodes of star formation (e.g., Mateo 1992; DaCosta 1992; Lehnert et al. 1992; Smecker-Hane et al. 1994).

Our new observations of NGC 1569 complement the recent optical survey by MHWS and the detailed optical study of NGC 1705 by Meurer et al. (1992) and reinforce their conclusions. Dwarf galaxies that are undergoing (or have recently experienced) major starbursts often exhibit large-scale expansion motions in their interstellar media that may ultimately result in the loss of a significant amount of gas and (especially) metals. The connection to starbursts means that these outflows are probably transient events. This may explain why flows of these sizes and velocities are not observed to be currently occurring in all star-forming low-mass galaxies (see Hunter et al. 1993). When they do occur, these outflows will likely have major consequences for the evolution of dwarf galaxies.

We thank the staff at the US *ROSAT* Science Data Center at the NASA/Goddard Space Flight Center for their help in introducing us to the joys and complexities of *ROSAT* and PROS. We also thank the staff of the Kitt Peak National Observatory for their help in obtaining the optical spectra discussed in this paper, and thank the staff in the SCARS division at STScI for their help in producing the astrometric overlays. We thank D. Balsara, D. De Young, M. Fall, C. Norman, A. Suchkov, M. Voit, B. Wang, and R. Wyse for helpful discussions about the theory of galactic winds and superbubbles. Thanks also to G. Bothun, H. Ferguson, J. Gallagher, C. Martin, and especially G. Meurer for enlightening conversations about dwarf galaxies. Special thanks to D. Hunter who kindly sent us her digital Hα image of this galaxy, to L. Drissen who likewise sent us his digital [O III] image of NGC 1569, and to C. Leitherer who provided detailed calculations of (and valuable advice concerning) starburst energetics. Finally, we thank the referee, G. Hensler, for his detailed and useful report. This research has made use of the NASA/IPAC Extragalactic Database (NED), which is operated by the Jet Propulsion Laboratory, Caltech, under contract with the National Aeronautics & Space Administration. T. H. and M. L. were supported in part by the NSF grant AST-90-20381, and T. H. and M. D. were also supported in part by the NASA grants NAGW-4025 and NAG5-1991. The work of M. L. at IGPP/LLNL was performed under the auspices of the US Department of Energy under contract W-7405-DNG-48.

REFERENCES

Ables, H. 1971, Publ. US Naval Obs., 20, no. 4, 61
Arimoto, N., & Yoshii, Y. 1986, A&A, 164, 260
Babul, A., & Rees, M. 1992, MNRAS, 255, 346
Berman, V., & Suchkov, A. 1991, Ap&SS, 184, 169
Binney, J., & Tremaine, S. 1987, Galactic Dynamics (Princeton: Princeton Univ. Press)
Bond, J. R., Szalay, A., & Silk, J. 1988, ApJ, 324, 627
Bothun, G., Mould, J., Caldwell, N., & MacGillivary, H. 1986, AJ, 92, 1007
Broadhurst, T., Ellis, R., & Glazebrook, K. 1992, Nature, 355, 55
Castor, J., McCray, R., & Weaver, R. 1975, ApJ, 200, L107
Chevalier, R., & Clegg, A. 1985, Nature, 317, 44
Da Costa, G. 1992, in IAU Symp. 149, The Stellar Populations of Galaxies, ed. B. Barbuy & A. Renzini (Dordrecht: Kluwer), 191
Dahlem, M., Lisenfeld, U., & Golla, G. 1995, ApJ, 444, 119
David, L., Harnden, F., Kearns, K., & Zombeck, M. 1993, The *ROSAT* High Resolution Imager (Cambridge: Harvard-Smithsonian Center for Astrophysics)
de Vaucouleurs, G. 1981, S&T, 62, 406
de Vaucouleurs, G., de Vaucouleurs, A., Corwin, H., Buta, R., Paturel, R., & Fouque, P. 1991, Third Reference Catalog of Bright Galaxies (Austin: Univ. Texas Press)
de Vaucouleurs, G., de Vaucouleurs, A., & Pence, W. 1974, ApJ, 194, L119
De Young, D., & Gallagher, J. 1990, ApJ, 356, L15
De Young, D., & Heckman, T. M. 1994, ApJ, 431, 598
Drissen, L., & Roy, J.-R. 1994, PASP, in press
Drissen, L., Roy, J.-R., & Moffat, A. 1993, AJ, 106, 1460

Elson, R., & Fall, S. M. 1988, AJ, 96, 1383
Fabbiano, G. 1988, ApJ, 330, 672
Fabbiano, G., Feigelson, E., & Zamorani, G. 1982, ApJ, 256, 397
Fabbiano, G., Kim, D.-W., & Trinchieri, G. 1992, ApJS, 80, 531
Faber, S., & Lin, D. 1983, ApJ, 266, L21
Gallagher, J., & Hunter, D. 1984, ARA&A, 22, 37
Griffiths, R., & Padovani, P. 1990, ApJ, 360, 483
Hartquist, T., & Dyson, J. 1993, QJRAS, 34, 57
Heckman, T., Lehnert, M., & Armus, L. 1993, in The Evolution of Galaxies and their Environments, ed. S. M. Shull & H. Thronson (Dordrecht: Kluwer), 455
Heiles, C. 1990, ApJ, 354, 483
Hensler, G., & Burkert, A. 1990, in Windows on Galaxies, ed. G. Fabbiano et al. (Dordrecht: Kluwer), 321
Hensler, G., Theis, C., & Burkert, A. 1993, in The Feedback of Chemical Evolution on the Stellar Content of Galaxies, ed. D. Alloin & G. Stasinska (Paris: l'Observatoire de Paris), 229
Hodge, P. 1974, ApJL, 191, L21
Hunter, D., & Gallagher, J. 1986, PASP, 98, 5
———. 1990, ApJ, 362, 480
Hunter, D., Gallagher, J., & Rautenkranz, D. 1982, ApJS, 49, 53
Hunter, D., Hawley, W., & Gallagher, J. 1993, AJ, 106, 1797
Hunter, D., Thronson, H., Casey, S., & Harper, A. 1989, ApJ, 341, 697
Israel, F. 1988, A&A, 194, 24
Israel, F., & de Bruyn, A. G. 1988, A&A, 198, 109
Israel, F., & van Driel, W. 1990, A&A, 236, 323
Kennicutt, R. 1992, ApJ, 388, 310
Kennicutt, R., & Kent, S. 1983, AJ, 88, 1094
Koo, B., & McKee, C. 1992, ApJ, 388, 103
Kormendy, J. 1985, ApJ, 295, 73
Larson, R. B. 1974, MNRAS, 169, 229
Larson, R. B., & Dinerstein, H. L. 1975, PASP, 87, 911
Lehnert, M. D., Bell, R., Hesser, J., & Oke, J. B. 1992, ApJ, 395, 466
Leitherer, C., & Heckman, T. 1995, ApJS, in press (LH)
Leitherer, C., Robert, C., & Drissen, L. 1992, ApJ, 401, 596
Lilly, S. 1993, ApJ, 411, 501
Long, K., Helfand, D., & Grabelsky, D. 1981, ApJ, 248, 925
Lynden-Bell, D. 1992, in Elements and the Cosmos, ed. M. Edmunds & R. Terlevich (Cambridge: Cambridge Univ. Press), 270
Mac Low, M., & McCray, R. 1988, ApJ, 324, 776
Marlowe, A., Heckman, T., Wyse, R., & Schommer, R. 1994, ApJ, 438, 563 (MHWS)
Mateo, M. 1992, in IAU Symp. 149, The Stellar Population of Galaxies, ed. B. Catbuy & A. Renzini (Dordrecht: Kluwer), 147
McKee, C., & Ostriker, J. 1977, ApJ, 218, 148
Maeder, A. 1990, A&AS, 84, 139
Meurer, G. 1989, Ph.D. thesis, Australian National Univ.
———. 1994, preprint
Meurer, G. Freeman, K., Dopita, M., & Cacciari, C. 1992, AJ, 103, 60
Miley, G. K. 1980, ARA&A, 18, 165
Nagase, F. 1989, PASJ, 41, 1
Norman, C., & Ikeuchi, S. 1989, ApJ, 345, 372
O'Connell, R., Gallagher, J., & Hunter, D. 1994, ApJ, 433, 65
Osterbrock, D. 1989, Astrophysics of Gaseous Nebulae and Active Galactic Nuclei (Mill Valley, CA: University Science Books)
Pagel, B., & Edmunds, M. 1981, ARA&A, 19, 77
Prada, F., Greve, A., & McKeith, C. 1994, A&A, 288, 396
Reakes, M. 1980, MNRAS, 192, 297
Roy, J.-R., Boulesteix, J., Joncas, J., & Grundseth, B. 1991, ApJ, 141
Saito, M. 1979, PASJ, 31, 193
Sandage, A. 1965, in The Structure & Evolution of Galaxies, 13th Solvay Institute, ed. H. Bondi (London: Interscience), 83
Sandage, A., & Binggeli, B. 1984, AJ, 89, 919
Schaaf, R., Pietsch, P., Biermann, P., Kronberg, P., & Schmutzler, T. 1989, ApJ, 336, 732
Schlegel, E. 1994, ApJ, 424, L99
Shu, F. 1991, The Physics of Astrophysics, Vol. 1, Radiation (Mill Valley, CA: University Science Books)
Shull, S. M., & McKee, C. 1979, ApJ, 227, 131
Shull, S. M., & Saken, J. 1995, ApJ, in press
Silk, J., Wyse, R. F. G., & Shields, G. 1987, ApJ, 322, L59
Skillman, E., Kennicutt, R., & Hodge, P. 1989, ApJ, 347, 875
Smecker-Hane, T., Stetson, P., Hesser, J., & Lehnert, M. 1994, preprint
Smith, R. C., Kirshner, R., Blair, W., & Winkler, P. F. 1991, ApJ, 375, 652
Sokolowski, J. 1995, ApJ, submitted
Stasinska, G. 1990, A&AS, 83, 501
Steidel, C. 1993, in The Environment & Evolution of Galaxies, ed. S. M. Shull & H. Thronson (Dordrecht: Kluwer), 263
Storchi-Bergman, T., Kinney, A., & Calzetti, D. 1995, ApJ, in press
Suchkov, A., Balsara, D., Heckman, T., & Leitherer, C. 1994, ApJ, 430, 511
Sutherland, R. 1993, ApJS, 88, 253
Tenario-Tagle, G., & Bodenheimer, P. 1988, ARA&A, 26, 145
Thuan, T., Izotov, Y., Lipovetsky, V., & Pustilnik, S. 1994, in Proc. Observatoire de Haute Provence Workshop on Dwarf Galaxies, in press
Tomisaka, K., & Bregman, J. 1993, PASJ, 45, 513
Tomisaka, K., & Ikeuchi, S. 1988, ApJ, 330, 695
Tomita, A., Ohta, K., & Saito, M. 1994, PASJ, 46, 335 (TOS)
Vader, J. P. 1986, ApJ, 305, 669
———. 1987, ApJ, 317, 128
Vaiana, G. 1990, in Imaging X-Ray Astronomy, ed. M. Elvis (Cambridge: Cambridge Univ. Press), 61
Waller, W. 1990, Ph.D. Dissertation, Univ. Massachusetts
———. 1991, ApJ, 370, 144
Waller, W., & Dracobl, C. 1993, in Massive Stars: Their Lives in the Interstellar Medium, ed. J. Cassinelli & E. Churchwell (ASP Conf. Series 35), 492
White, S., & Frenk, S. 1991, ApJ, 379, 52
Wilcots, E., Puche, D., Waller, W., & Westpfahl, D. 1995, in preparation